rected movement: in vitro motile properties of fission yeast kinesin-14 Pkl1. J Biol Chem 283:36465–36473.
Goedert M, Jakes R, Vanmechelen E (1995) Monoclonal antibody AT8 recognises tau protein phosphorylated at both serine 202 and threonine 205. Neurosci Lett 189:167–169.
Hagiwara H, Yorifuji H, Sato-Yoshitake R, Hirokawa N (1994) Competition between motor molecules (kinesin and cytoplasmic dynein) and fibrous microtubule-associated proteins in binding to microtubules. J Biol Chem 269:3581–3589.
Hanger DP, Anderton BH, Noble W (2009) Tau phosphorylation: the therapeutic challenge for neurodegenerative disease. Trends Mol Med 15:112–119.
Hisanaga S, Hirokawa N (1989) The effects of dephosphorylation on the structure of the projections of neurofilament. J Neurosci 9:959–966.
Hollenbeck PJ, Saxton WM (2005) The axonal transport of mitochondria. J Cell Sci 118:5411–5419.
Hosokawa T, Saito T, Asada A, Fukunaga K, Hisanaga S (2010) Quantitative measurement of in vivo phosphorylation states of Cdk5 activator p35 by Phos-tag SDS-PAGE. Mol Cell Proteomics 9:1133–1143.
Ishiguro K, Takamatsu M, Tomizawa K, Omori A, Takahashi M, Arioka M, Uchida T, Imahori K (1992) Tau protein kinase I converts normal tau protein into A68-like component of paired helical filaments. J Biol Chem 267:10897–10901.
Jeganathan S, von Bergen M, Brutlach H, Steinhoff HJ, Mandelkow E (2006) Global hairpin folding of tau in solution. Biochemistry 45:2283–2293.
Jeganathan S, Hascher A, Chinnathambi S, Biernat J, Mandelkow EM, Mandelkow E (2008) Proline-directed pseudo-phosphorylation at AT8 and PHF1 epitopes induces a compaction of the paperclip folding of tau and generates a pathological (MC-1) conformation. J Biol Chem 283:32066–32076.
Jicha GA, Bowser R, Kazam IG, Davies P (1997) Alz-50 and MC-1, a new monoclonal antibody raised to paired helical filaments, recognize conformational epitopes on recombinant tau. J Neurosci Res 48:128–132.
Jicha GA, Berenfeld B, Davies P (1999) Sequence requirements for formation of conformational variants of tau similar to those found in Alzheimer's disease. J Neurosci Res 55:713–723.
Kaminosono S, Saito T, Oyama F, Ohshima T, Asada A, Nagai Y, Nukina N, Hisanaga S (2008) Suppression of mutant Huntingtin aggregate formation by Cdk5/p35 through the effect on microtubule stability. J Neurosci 28:8747–8755.
Kanai Y, Takemura R, Oshima T, Mori H, Ihara Y, Yanagisawa M, Masaki T, Hirokawa N (1989) Expression of multiple tau isoforms and microtubule bundle formation in fibroblasts transfected with a single tau cDNA. J Cell Biol 109:1173–1184.
Kanungo J, Zheng Y, Rudrabhatla P, Amin N, Mishra B, Pant H (2011) Deregulation of cytoskeletal protein phosphorylation and neurodegeneration. In: Advances in neurobiology: cytoskeleton of the nervous system (Nixon RA and Yuan A, eds), pp 297–324. New York: Springer.
Kimura T, Yamashita S, Fukuda T, Park JM, Murayama M, Mizoroki T, Yoshiike Y, Sahara N, Takashima A (2007) Hyperphosphorylated tau in parahippocampal cortex impairs place learning in aged mice expressing wild-type human tau. EMBO J 26:5143–5152.
Kinoshita E, Kinoshita-Kikuta E, Takiyama K, Koike T (2006) Phosphate-binding tag, a new tool to visualize phosphorylated proteins. Mol Cell Proteomics 5:749–757.
Knowles R, LeClerc N, Kosik KS (1994) Organization of actin and microtubules during process formation in tau-expressing Sf9 cells. Cell Motil Cytoskeleton 28:256–264.
Kumar S, Yin X, Trapp BD, Hoh JH, Paulaitis ME (2002) Relating interactions between neurofilaments to the structure of axonal neurofilament distributions through polymer brush models. Biophys J 82:2360–2372.
Lippens G, Sillen A, Landrieu I, Amniai L, Sibille N, Barbier P, Leroy A, Hanoulle X, Wieruszeski JM (2007) Tau aggregation in Alzheimer's disease: what role for phosphorylation? Prion 1:21–25.
Liu F, Li B, Tung EJ, Grundke-Iqbal I, Iqbal K, Gong CX (2007) Site-specific effects of tau phosphorylation on its microtubule assembly activity and self-aggregation. Eur J Neurosci 26:3429–3436.
Mandelkow EM, Thies E, Trinczek B, Biernat J, Mandelkow E (2004) MARK/PAR1 kinase is a regulator of microtubule-dependent transport in axons. J Cell Biol 167:99–110.
Marx A, Pless J, Mandelkow EM, Mandelkow E (2000) On the rigidity of the cytoskeleton: are MAPs cross-linkers or spacers of microtubules? Cell Mol Biol 46:949–965.
Marx A, Müller J, Mandelkow EM, Hoenger A, Mandelkow E (2006) Interaction of kinesin motors, microtubules, and MAPs. J Muscle Res Cell Motil 27:125–137.
Morel, M, Authelet M, Dedecker R, Brion JP (2010) Glycogen synthase kinase-3 and the P25 activator of cyclin dependent kinase 5 increase pausing of mitochondria in neurons. Neuroscience 167:1044–1056.
Morishima-Kawashima M, Hasegawa M, Takio K, Suzuki M, Yoshida H, Titani K, Ihara Y (1995) Proline-directed and non-proline-directed phosphorylation of PHF-tau. J Biol Chem 270:823–829.
Mukhopadhyay R, Hoh JH (2001) AFM force measurements on microtubule-associated proteins: the projection domain exerts a long-range repulsive force. FEBS Lett 505:374–378.
Planel E, Sun X, Takashima A (2002) Role of GSK-3β in Alzheimer's disease pathology. Drug Dev Res 56:491–510.
Plattner F, Angelo M, Giese KP (2006) The roles of cyclin-dependent kinase 5 and glycogen synthase kinase 3 in tau hyperphosphorylation. J Biol Chem 281:25457–25465.
Rankin CA, Sun Q, Gamblin TC (2005) Pseudo-phosphorylation of tau at Ser202 and Thr205 affects tau filament formation. Mol Brain Res 138:84–93.
Rochlin MW, Wickline KM, Bridgman PC (1996) Microtubule stability decreases axon elongation but not axoplasm production. J Neurosci 16:3236–3246.
Rudrabhatla P, Grant P, Jaffe H, Strong MJ, Pant HC (2010) Quantitative phosphoproteomic analysis of neuronal intermediate filament proteins (NF-M/H) in Alzheimer's disease by iTRAQ. FASEB J 24:4396–4407.
Saito T, Onuki R, Fujita Y, Kusakawa G, Ishiguro K, Bibb JA, Kishimoto T, Hisanaga S (2003) Developmental regulation of the proteolysis of the p35 cyclin-dependent kinase 5 activator by phosphorylation. J Neurosci 23:1189–1197.
Sakaue F, Saito T, Sato Y, Asada A, Ishiguro K, Hasegawa M, Hisanaga S (2005) Phosphorylation of FTDP-17 mutant tau by cyclin-dependent kinase 5 complexed with p35, p25, or p39. J Biol Chem 280:31522–31529.
Seeger MA, Rice SE (2010) Microtubule-associated protein-like binding of the kinesin-1 tail to microtubules. J Biol Chem 285:8155–8162.
Shahpasand K, Ahmadian S, Riazi GH (2008) A possible mechanism for controlling processive transport by microtubule-associated proteins. Neurosci Res 61:347–350.
Shemesh OA, Erez H, Ginzburg I, Spira ME (2008) Tau-induced traffic jams reflect organelles accumulation at points of microtubule polar mismatching. Traffic 9:458–471.
Stamer K, Vogel R, Thies E, Mandelkow E, Mandelkow EM (2002) Tau blocks traffic of organelles, neurofilaments, and APP-vesicles in neurons and enhances oxidative stress. J Cell Biol 156:1051–1063.
Stokin GB, Lillo C, Falzone TL, Brusch RG, Rockenstein E, Mount SL, Raman R, Davies P, Masliah E, Williams DS, Goldstein LS (2005) Axonopathy and transport deficits early in the pathogenesis of Alzheimer's disease. Science 307:1282–1288.
Stoothoff WH, Johnson GV (2005) Tau phosphorylation: physiological and pathological consequences. Biochim Biophys Acta 1739:280–297.
Stoothoff W, Jones PB, Spires-Jones TL, Joyner D, Chhabra E, Bercury K, Fan Z, Xie H, Bacskai B, Edd J, Irimia D, Hyman BT (2009) Differential effect of three-repeat and four-repeat tau on mitochondrial axonal transport. J Neurochem 111:417–427.
Su B, Wang X, Zheng L, Perry G, Smith MA, Zhu X (2010) Abnormal mitochondrial dynamics and neurodegenerative diseases. Biochim Biophys Acta 1802:135–142.
Sudo H, Baas PW (2010) Acetylation of microtubules influences their sensitivity to severing by katanin in neurons and fibroblasts. J Neurosci 30:7215–7226.
Takahashi S, Saito T, Hisanaga S, Pant HC, Kulkarni AB (2003) Tau phosphorylation by cyclin-dependent kinase 5/p39 during brain development reduces its affinity for microtubules. J Biol Chem 278:10506–10515.
Tatebayashi Y, Haque N, Tung YC, Iqbal K, Grundke-Iqbal I (2004) Role of tau phosphorylation by glycogen synthase kinase-3W in the regulation of organelle transport. J Cell Sci 117:1653–1663.
Thies E, Mandelkow EM (2007) Missorting of tau in neurons causes degeneration of synapses that can be rescued by MARK2/Par-1. J Neurosci 27:2896–2907.

Tokuoka H, Saito T, Yorifuji H, Wei F, Kishimoto T, Hisanaga S (2000) Brain-derived neurotrophic factor-induced phosphorylation of neurofilament-H subunit in primary cultures of embryo rat cortical neurons. J Cell Sci 113:1059–1068.

Trinczek B, Ebneth A, Mandelkow EM, Mandelkow E (1999) Tau regulates the attachment/detachment but not the speed of motors in microtubule-dependent transport of single vesicles and organelles. J Cell Sci 112:2355–2367.

Uchida A, Tashiro T, Komiya Y, Yorifuji H, Kishimoto T, Hisanaga S (2004) Morphological and biochemical changes of neurofilaments in aged rat sciatic nerve axons. J Neurochem 88:735–745.

Vershinin M, Carter BC, Razafsky DS, King SJ, Gross SP (2007) Multiple motor based transport and its regulation by Tau. Proc Natl Acad Sci U S A 104:87–92.

Vershinin M, Xu J, Razafsky DS, King SJ, Gross SP (2008) Tuning microtubule-based transport through flamentous MAPs: the problem of dynein. Traffic 9:882–892.

Verwer RW, Sluiter AA, Balesar RA, Baayen JC, Noske DP, Dirven CM, Wouda J, van Dam AM, Lucassen PJ, Swaab DF (2007) Mature astrocytes in the adult human neocortex express the early neuronal marker doublecortin. Brain 130:3321–3335.

Vossel KA, Zhang K, Brodbeck J, Daub AC, Sharma P, Finkbeiner S, Cui B, Mucke L (2010) Tau reduction prevents Abeta-induced defects in axonal transport. Science 330:198.

Wada Y, Ishiguro K, Itoh TJ, Uchida T, Hotani H, Saito T, Kishimoto T, Hisanaga S (1998) Microtubule-stimulated phosphorylation of tau at Ser202 and Thr205 by cdk5 decreases its microtubule nucleation activity. J Biochem 124:738–746.

Wang ZF, Li HL, Li XC, Zhang Q, Tian Q, Wang Q, Xu H, Wang JZ (2006) Effects of endogenous beta-amyloid overproduction on tau phosphorylation in cell culture. J Neurochem 98:1167–1175.

Watanabe A, Hasegawa M, Suzuki M, Takio K, Morishima-Kawashima M, Titani K, Arai T, Kosik KS, Ihara Y (1993) In vivo phosphorylation sites in fetal and adult rat tau. J Biol Chem 268:25712–25717.

Yu W, Baas PW (1994) Changes in microtubule number and lenghh during axon differentiation. J Neurosci 14:2818–2829.

OPEN ACCESS Freely available online

PLOS | ONE

Methylene Blue Reduced Abnormal Tau Accumulation in P301L Tau Transgenic Mice

Masato Hosokawa[1], Tetsuaki Arai[1,2], Masami Masuda-Suzukake[3], Takashi Nonaka[3], Makiko Yamashita[3], Haruhiko Akiyama[1]*, Masato Hasegawa[3]

1 Department of Dementia and Higher Brain Function, Tokyo Metropolitan Institute of Medical Science, Tokyo, Japan, **2** Department of Psychiatry, Graduate School of Comprehensive Human Sciences, University of Tsukuba, Tsukuba, Japan, **3** Department of Pathology and Cell Biology, Tokyo Metropolitan Institute of Medical Science, Tokyo, Japan

Abstract

In neurodegenerative disorders, abnormally hyperphosphorylated and aggregated tau accumulates intracellularly, a mechanism which is thought to induce neuronal cell death. Methylene blue, a type of phenothiazine, has been reported to inhibit tau aggregation in vitro. However, the effect of methylene blue in vivo has remained unknown. Therefore, we examined whether methylene blue suppresses abnormal tau accumulation using P301L tau transgenic mice. At 8 to 11 months of age, these mice were orally administered methylene blue for 5 months. Subsequent results of Western blotting analysis revealed that this agent reduced detergent-insoluble phospho-tau. Methylene blue may have potential as a drug candidate for the treatment of tauopathy.

Citation: Hosokawa M, Arai T, Masuda-Suzukake M, Nonaka T, Yamashita M, et al. (2012) Methylene Blue Reduced Abnormal Tau Accumulation in P301L Tau Transgenic Mice. PLoS ONE 7(12): e52389. doi:10.1371/journal.pone.0052389

Editor: Andrea C. LeBlanc, McGill University, Canada

Received June 12, 2012; **Accepted** November 14, 2012; **Published** December 20, 2012

Funding: This research was partially supported by the Japan Society for the Promotion of Science, Grants-in-Aid for Scientific Research (C), grant number 21591536 to HA and 24591738 to M. Hosokawa. The additional part of the funding of the authors' study has come from institute budget. The funders had no role in study design, data collection and analysis, decision to publish, or preparation of the manuscript.

Competing Interests: The authors have declared that no competing interests exist.

* E-mail: akiyama-hr@igakuken.or.jp

Introduction

In neurodegenerative disorders such as Alzheimer's disease, corticobasal degeneration, and supranuclear palsy, the microtubule–associated protein tau is abnormally phosphorylated and redistributed into paired helical filaments (PHFs) forming neurofibrillary tangles, a process that correlates with pyramidal cell destruction and dementia. Abnormal tau accumulation is characterized by hyperphosphorylation, conformational change and aggregation with changes in solubility.

Wischik et al. have identified a nonneuroleptic phenothiazine which reverses the proteolytic stability of protease-resistant PHFs by blocking tau-tau binding through the repeat domain [1]. Moreover, phenothiazines, including methylthioninium chloride (methylene blue (MB)), polyphenols and porphyrins, inhibited heparin-induced tau filament formation in vitro [2]. Based on these results, tau aggregation inhibitors are considered to be strong candidates for the treatment of tauopathy.

TauRx Pharmaceuticals recently announced the completion of MB phase II clinical trials. They conducted MB dosing and efficacy studies involving 321 people with mild to moderate Alzheimer's disease. Over a 50-week period, the cognitive decline of those on the drug appeared to be 81% slower than those taking a placebo. These results were presented at a conference [3] but have not been published. Currently, a large-scale phase III trial is in planning [4].

To date, there are two reports on the effect of MB on tau aggregation in vivo. In one study, MB did not alter abnormal tau phosphorylation and failed to inhibit tau-dependent neuronal cell toxicity in zebrafish [5]. The other study employed a distinct tau transgenic mouse line and mice received a 2–3-week treatment with oral MB. In this latter study, MB acted as a tau aggregation inhibitor. Although, these findings have been described in brief in a conference abstract, the details are unavailable [6].

More recently, Congdon et al. demonstrated that MB could induce autophagy in primary neurons, organotypic slice cultures and tau transgenic mice (JNPL3) [7]. They also showed a 2 week oral administration of MB attenuated the total tau levels in the absence of significant changes in sarkosyl-insoluble tau levels.

In the present study, we investigated whether MB could reduce abnormal tau accumulation by carrying out long-term oral administration of MB using tau transgenic mice with the P301L mutation as a tauopathy model. Our results suggested that oral intake of MB could be a potential treatment for tauopathy.

Materials and Methods

Ethics Statement

This study was carried out in strict accordance with the recommendations provided in the Guide for the Care and Use of Laboratory Animals of the Ministry of Health, Labour and Welfare of Japan and the Ministry of Education, Culture, Sports, Science and Technology of Japan. The protocol was approved by the Committee on the Ethics of Animal Experiments of the Tokyo Metropolitan Institute of Medical Science (Permit Numbers: 22–23 and 11-028). All experiments were performed under sodium pentobarbital anesthesia and every effort was made to minimize suffering.

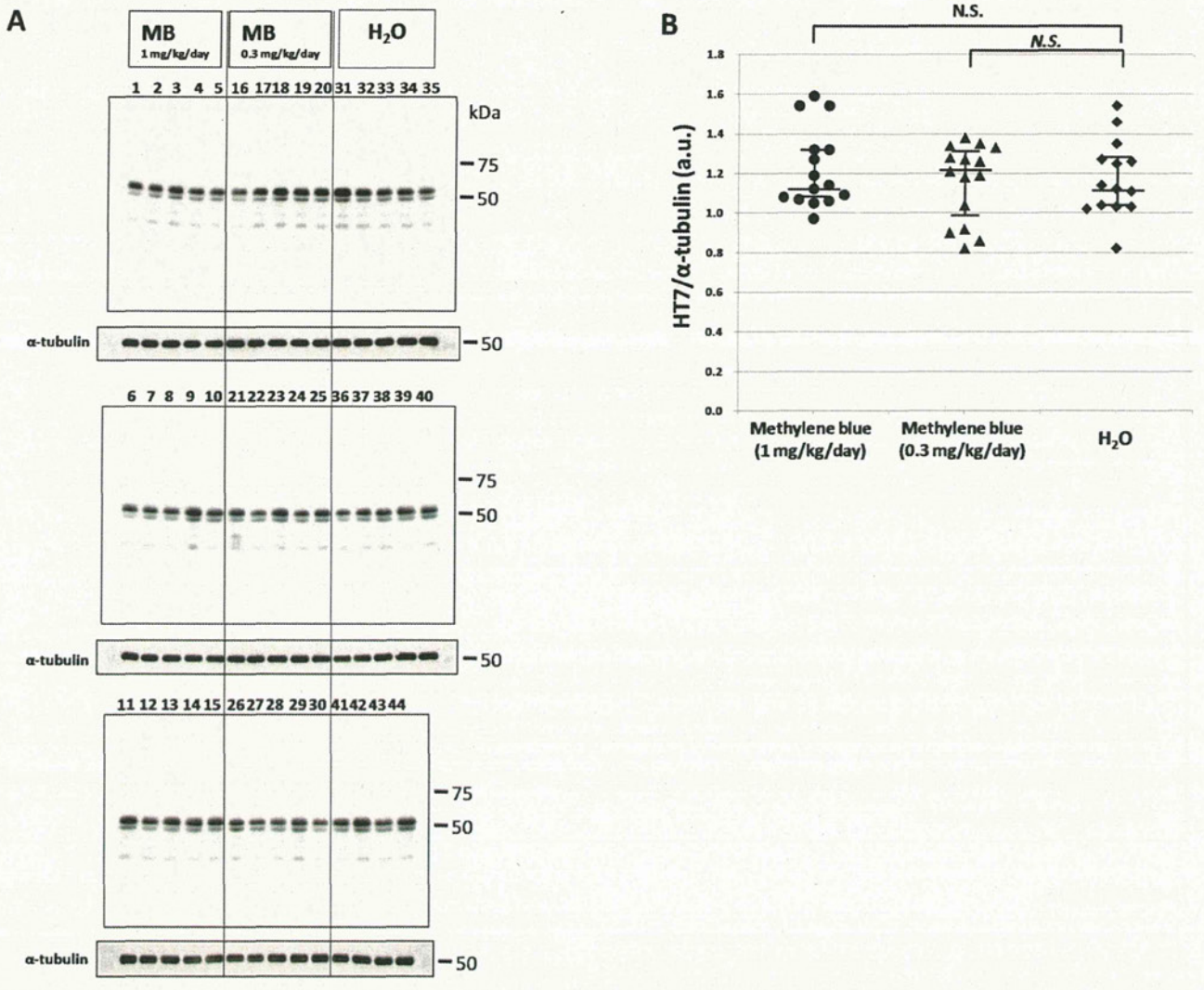

Figure 1. Immunoblotting analysis of total tau in the Tris-soluble fraction. (A) Immunoblotting analysis was visualized using HT7 antibody for the Tris-soluble fraction. The numbers indicate individual mice: 1–15, MB 1 mg/kg/day group; 16–30, MB 0.3 mg/kg/day group; and 31–44, water only group. Molecular weight markers are shown on the right (kDa). For quantitative measure of band intensity, α-tubulin was used as an internal control for protein concentration. (B) A comparison of the relative total tau (HT7) expression levels of the MB-treated groups and the water only group. The data were compared with the HT7 band intensity, which was normalized with α-tubulin. The central lines indicate medians and the vertical lines represent 25th and 75th percentiles. a.u., arbitrary unit. N.S., no significant difference.
doi:10.1371/journal.pone.0052389.g001

Animals

P301L tau transgenic mice (JNPL3) [8] were purchased from Taconic (USA) via IBL (Japan). The experiments utilized 44 female hemizygote tau mice. The mice were reared in the animal facility of Tokyo Metropolitan Institute of Medical Science under standard conditions at 24±2°C and were maintained on a commercial diet supplied ad libitum.

The transgenic mice [8] aged 8–11 months were divided into 3 groups: the first group (14 mice) was given water alone, the second group (15 mice) was given water containing 2 μg/ml MB and the third group (15 mice) was given water containing 6 μg/ml MB. All were maintained on their respective regimens for 5 months. The daily MB intake was estimated to be about 0.3 or 1 mg/kg/day per mouse, on the assumption that a mouse weighs 30 g and takes in 5 ml of water a day.

At the end of the experimental period, mice were sacrificed under quick anesthesia with 200 mg/kg body weight of sodium pentobarbital delivered intraperitoneally and their brains were quickly removed. Brains of each group were cut along the sagittal plane and the left hemisphere was frozen and stored at −80°C for biochemical analyses. The right hemisphere was fixed in 4% paraformaldehyde in 0.1 M phosphate buffer for 48 hours in the cold. Brain blocks were then transferred to a maintenance solution of 15% sucrose in 0.01 M phosphate-buffered saline (PBS), pH 7.4.

Analysis of Tau Deposition

Deposition of tau was analyzed using immunohistochemical staining with AT8 antibody (recognizes phosphorylation at both serine 202 and threonine 205) and MC-1 antibody. Biotinylation of MC-1 antibody was performed using a Zenon Mouse IgG

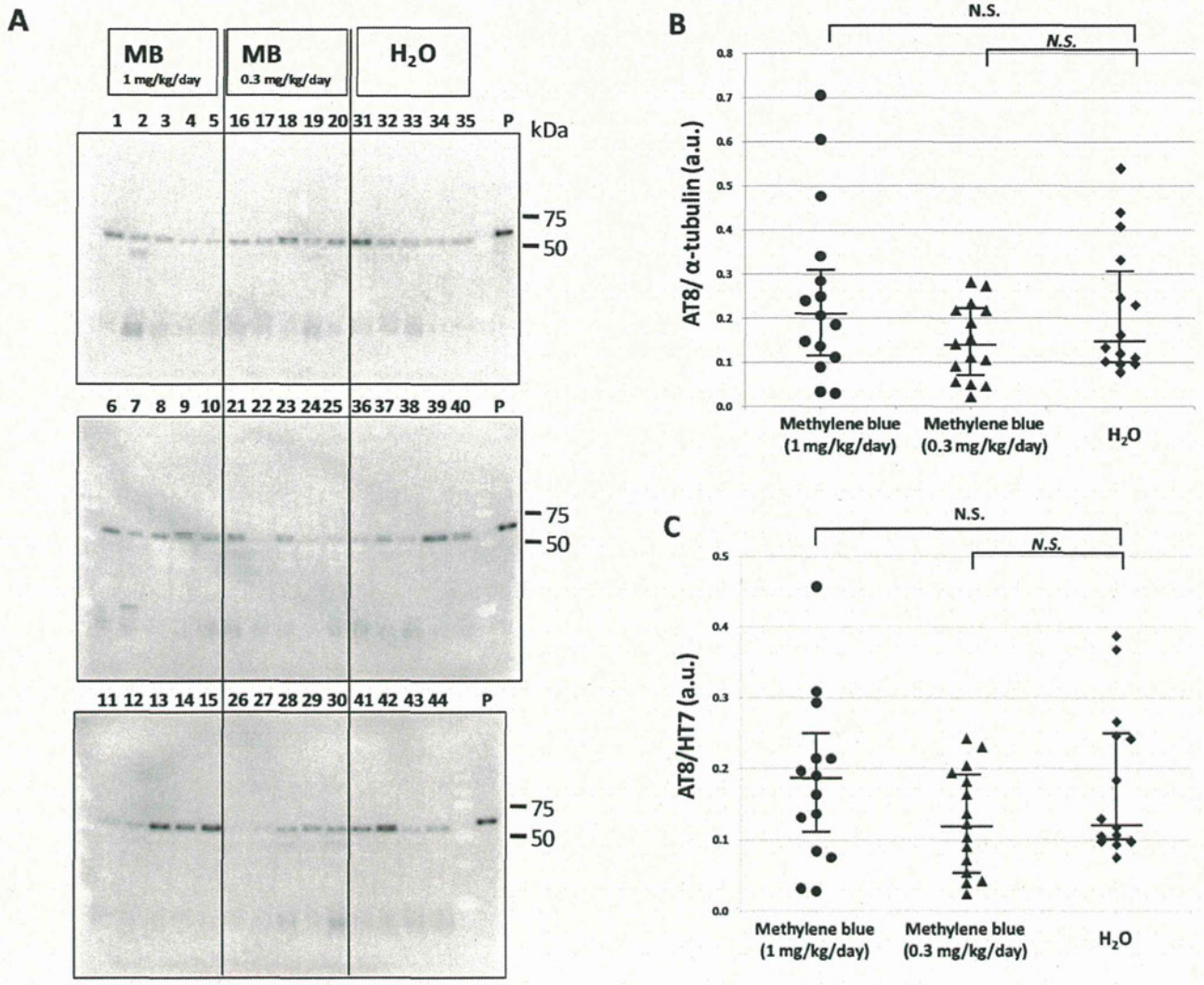

Figure 2. Immunoblotting analysis of phosphorylated tau in the Tris-soluble fraction. (A) Immunoblot analysis was visualized using AT8 antibody for the Tris-soluble fraction. The numbers indicate individual mice: 1–15, MB 1 mg/kg/day group; 16–30, MB 0.3 mg/kg/day group; and 31–44, water only group. Molecular weight markers are shown on the right (kDa). P, positive control (P301L tau transgenic mouse, 20 month-old female). (B) A comparison of relative phosphorylated tau (AT8) expression levels of the MB-treated groups and the water only group. The data were compared with the AT8 band intensity, which was normalized with α-tubulin. (C) A comparison of the relative phosphorylated tau (AT8)/total tau (HT7) levels of the MB-treated groups and the water only group. The data were compared with the AT8 band intensity, which was normalized with the total tau (HT7) band intensity. The central lines indicate medians and the vertical lines represent 25th and 75th percentiles. a.u., arbitrary unit. N.S., no significant difference.
doi:10.1371/journal.pone.0052389.g002

Labeling Kit (Molecular Probes, Inc. Eugene, OR, USA) according to the manufacturer's instructions. For immunohistochemistry, sagittal sections were cut serially on a freezing microtome at 30 μm thickness, collected in the maintenance solution, and immunostained as free-floating sections. Following a pretreatment with 0.5% H_2O_2 for 30 min to eliminate endogenous peroxidase activity, sections were incubated for 72 hours with AT8 antibody (Biotinylated-AT8, 1:1,000, Innogenetics, Ghent, Belgium) or overnight with biotinylated MC-1 antibody (1:100, a generous gift of Dr. Davies) [9] diluted in PBS containing 0.3% Triton X-100 (PBS-Tx). The antibody labeling was visualized by incubation with avidin-biotinylated horseradish peroxidase (HRP) complex (ABC Elite, 1:1,000, Vector Laboratories, Burlingame, CA, USA) for 3 hours, followed by incubation with a solution containing 0.01% 3,3′-diaminobenzidine (DAB), 1% nickel ammonium sulfate, 0.05 M imidazole and 0.00015% H_2O_2 in 0.05 M Tris-HCl buffer, pH 7.6. Counter nuclear staining was performed with Kernechtrot stain solution (Merck, Darmstadt, Germany). The sections were then rinsed with distilled water, mounted on glass slides, treated with Xylene, and coverslipped with Entellan (Merck). Photographs were taken with an Olympus VS120-S5 (Olympus, Tokyo, Japan) or a BX51 microscope (Olympus).

Sequential Fractionation of Brain Extracts

Frozen left hemispheres (approximately, 0.2 g) were homogenized in 10 volumes of buffer H (10 mM Tris-HCl, pH 7.5, 0.8 M NaCl, 1 mM ethylene glycol bis-N, N, N', N'-tetraacetic acid, 1 mM dithiothreitol). The hemisphere included the olfactory bulb, cerebral cortex, striatum, thalamus, hypothalamus, cerebellum,

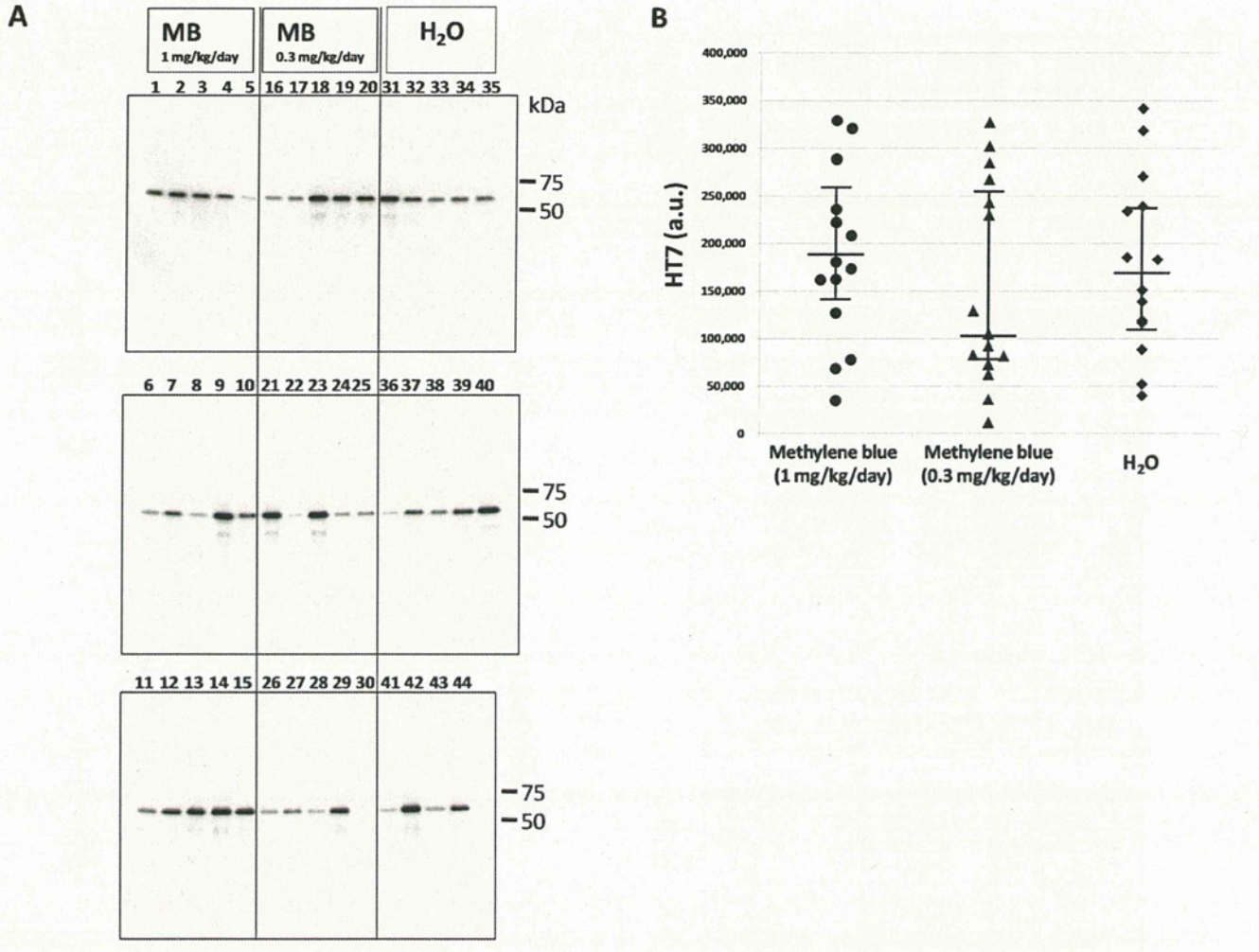

Figure 3. Immunoblotting analysis of total tau in the sarkosyl-insoluble fraction. (A) Immunoblot analysis was visualized using HT7 antibody for the sarkosyl-insoluble fraction. The numbers indicate individual mice: 1–15, MB 1 mg/kg/day group; 16–30, MB 0.3 mg/kg/day group; 31–44, water only group. Molecular weight markers are shown on the right (kDa). (B) A comparison of relative total tau (HT7) expression levels in the sarkosyl-insoluble fraction of the MB-treated groups and the water only group. The data were compared with the HT7 band intensity. The central lines indicate medians and the vertical lines represent 25th and 75th percentiles. a.u., arbitrary unit.
doi:10.1371/journal.pone.0052389.g003

midbrain, pons, medulla oblongata and the upper part of the spinal cord. The method used for sequential fractionation of brain extracts was originally described by Greenberg et al. [10]. Briefly, the brain homogenate was centrifuged at 100,000×g for 20 min at 4°C, and the supernatants were collected as the Tris-soluble fraction. The resultant pellet was homogenized in 10 volumes of buffer H, followed by an incubation for 30 min at 37°C with 1% Triton X-100. The homogenate was then centrifuged at 100,000×g for 20 min at 4°C. The Triton X-100 insoluble pellet was sonicated in 5 volumes of buffer H containing 1% sarkosyl and centrifuged at 100,000×g for 20 min at 4°C. The pellet was then sonicated in 1 volume of SDS-PAGE sample buffer.

Immunoblotting Analysis

For immunoblotting, brain extracts from the tau mice were boiled for 5 minutes with SDS-PAGE sample buffer (60 mM Tris-HCl, pH 6.8, containing 2% SDS, 10% glycerol, 0.025% bromophenol blue and 5% mercaptoethanol) and loaded onto a 10% acrylamide minigel. Loaded samples were electrophoresed for 45 minutes at 200 V with molecular weight markers (Bio-Rad, Hercules, CA, USA). Electrophoresed proteins were transferred onto a polyvinylidene difluoride membrane (Millipore, Billerica, MA, USA) for 60 minutes at 200 mA. The printed membranes were blocked with 3% gelatin for 1 hour and then incubated in a primary antibody solution (HT7, 1:3,000, Innogenetics, AT8, 1:3,000, Innogenetics, or anti-α-tubulin, 1:10,000, Sigma, St. Louis, MO, USA) overnight at room temperature. Following incubation with a secondary antibody (1:20,000, Bio-Rad), immunoreactivity was detected by the chemiluminescence method using an ECL plus Western Blotting Detection Kit (GE Healthcare UK Ltd., Buckinghamshire, England) or SuperSignal West Dura Extended Duration Substrate (Pierce, Rockford IL, USA) and was visualized with LAS-3000 (Fujifilm, Tokyo, Japan). For quantitative measure of band intensity, α-tubulin was used as an internal control for protein concentration.

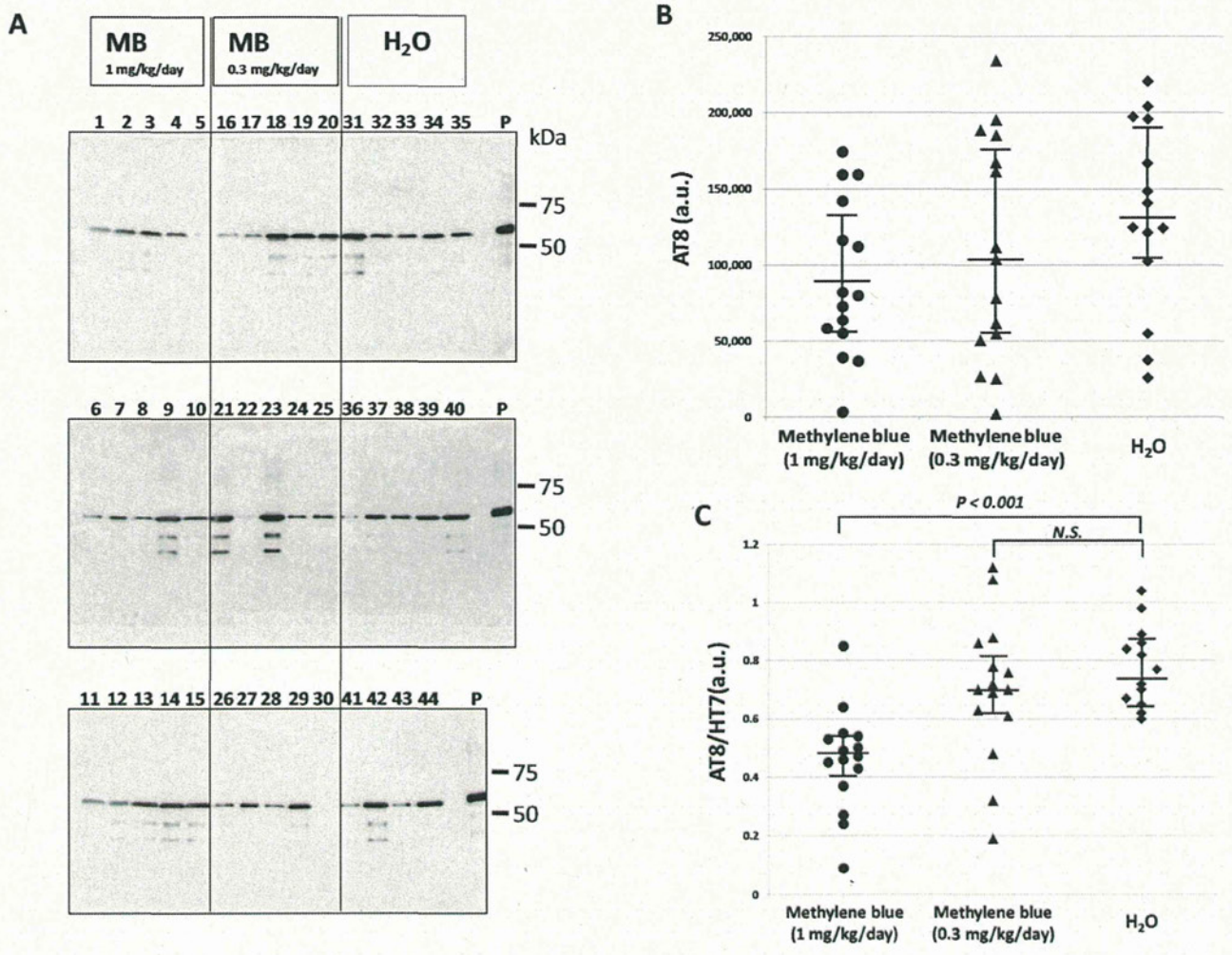

Figure 4. Immunoblotting analysis of abnormal tau in the sarkosyl-insoluble fraction. (A) Immunoblotting analysis was visualized using AT8 antibody for the sarkosyl-insoluble fraction. The numbers indicate individual mice: 1–15, MB 1 mg/kg/day group; 16–30, MB 0.3 mg/kg/day group; and 31–44, water only group. Molecular weight markers are shown on the right (kDa). P, positive control (P301L tau transgenic mouse, 20 month-old female). (B) A comparison of relative AT8 expression levels of the MB-treated groups and the water only group. The data were compared with the AT8 band intensity. (C) A comparison of relative phosphorylated tau (AT8)/total tau (HT7) levels of the MB-treated groups and the water only group. The data were compared with the AT8 band intensity, which was normalized with the total tau (HT7) band intensity. The central lines indicate medians and the vertical lines represent 25th and 75th percentiles. $P<0.01$ was considered to represent a statistically significant difference. a.u., arbitrary unit. N.S., no significant difference.
doi:10.1371/journal.pone.0052389.g004

Statistical Analyses

The data are presented as medians (interquartile range) [range]. The significance of difference between values was estimated by means of Kruskal-Wallis analysis of variances with post hoc Steel's method. $P<0.05$ was considered to indicate a statistically significant difference.

Results

Immunoblotting Analysis

To investigate the effect of methylene bule on tau accumulation, P301L tau transgenic mice were administered MB for 5 months starting at 8–11 months of age. Brains were then collected and sequential protein extraction and immunoblotting were performed (Figs. 1, 2, 3, 4). Total tau in the Tris-soluble fraction was detected by HT7 antibody (Fig. 1A), and there were no prominent differences among the three groups by quantitative analysis of band intensities, which was normalized with α-tubulin (Fig. 1B). Phosphorylated tau in the Tris-soluble fraction was also detected by AT8 antibody (Fig. 2A). The data were compared with the AT8 band intensity, which was normalized with α-tubulin (Fig. 2B) or with the total tau (HT7) band intensity (Fig. 2C). There were also no significant differences in phosphorylated tau in the Tris-soluble fraction among the three groups (Figs. 2B and 2C).

Phosphorylated tau and total tau in the sarkosyl-insoluble fraction were visualized again by Western blotting using HT7 antibody (Fig. 3A) and AT8 (Fig. 4A), respectively. The HT7 (Fig. 3B) and AT8 (Fig. 4B) band intensities were measured. Then, we compared the AT8 band intensity normalized by the total tau (HT7) band intensity and were expressed as medians (interquartile range) [range]. The AT8/HT7 ratio was 0.47 (0.40–0.53) [0.09–0.85] (n = 15) in the MB group given 1 mg/kg/day, 0.70 (0.62–0.82) [0.19–1.12] (n = 15) in the MB group given 0.3 mg/kg/day, and 0.74 (0.65–0.86) [0.60–1.04] (n = 14) in the group given water

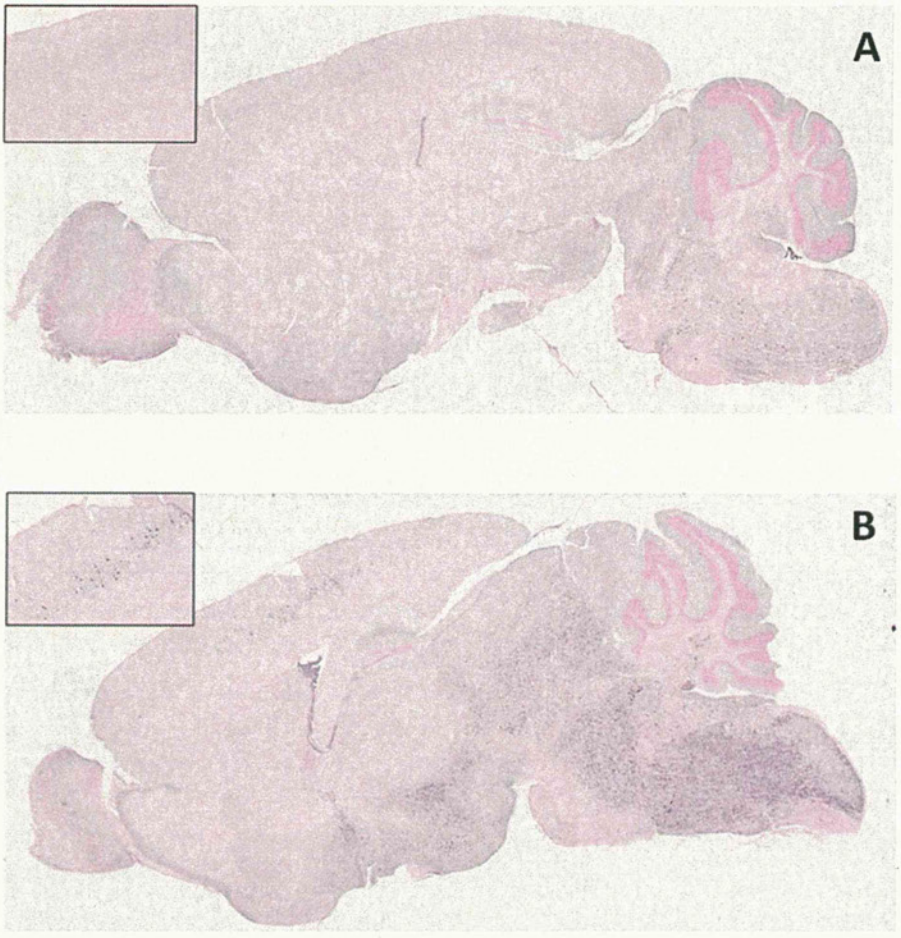

Figure 5. Immunohistochemical staining of abnormal tau. (A) An AT8 immunoreaction was observed only in spinal cord, medulla oblongata and pons of a mouse with a low AT8/HT7 ratio. (B) AT8-positive cells were seen in spinal cord, medulla oblongata, pons, midbrain, hypothalamus and cerebral cortex of a mouse with a high AT8/HT7 ratio. Each insert shows the cerebral cortex of the mouse brain.
doi:10.1371/journal.pone.0052389.g005

alone (Fig. 4C). The Kruskal-Wallis test followed by Steel's multiple comparison test was used for statistical analyses, and there was a significant difference between the group given MB 1 mg/kg/day and the group given water alone ($P<0.001$). There was no significant difference between the 0.3 mg/kg/day group and the water only group ($P = 0.422$). Immunoblotting analysis revealed that the level of abnormally phosphorylated tau accumulation was decreased in the P301L tau mice given MB as compared with the P301L tau mice given water alone.

Analysis of Tau Deposition

A weak AT8 immunoreaction was observed only in the spinal cord, medulla oblongata and pons of the mice with a low AT8/HT7 ratio (Fig. 5A). On the other hand, AT8-positive cells were seen in the spinal cord, medulla oblongata, cerebellar nuclei, pons, midbrain, hypothalamus and primary motor cortex of mice with a high AT8/HT7 ratio (Fig. 5B). Immunohistochemical staining with a conformational antibody, MC-1, which recognizes aggregated tau showed that MC-1-positive neurons and cellular processes were seen in the motor cortex, hypothalamus and pons (Fig. 6). However, MC-1-positive neurons and cellular processes in these areas of mice with a low AT8/HT7 ratio were significantly fewer than those in mice with a high AT8/HT7 ratio.

Discussion

Cases of dementia including AD have been increasing in number in recent years, and discovering effective drugs for treating these diseases must be facilitated. Developing a novel drug for the treatment of AD is a time-consuming process and a better approach might be through screening chemical compounds or drugs which are already available. Consequently, we evaluated MB inhibition of abnormal tau accumulation using a tauopathy mouse model, since MB had been shown to be a protein aggregation inhibitor *in vitro* [2] as well as more recently in cells [11].

MB was found to have an inhibitory effect on tau aggregation *in vitro* [1–2] and to act as a tau aggregation inhibitor in a cellular model as well as in transgenic mice [6]. However, in the latter case, only an abstract was published on these findings and the details were unavailable. More recently, Congdon et al. reported that MB induced autophagy and attenuated tauopathy in vitro and in vivo [7]. They administrated MB (0.02, 2, and 20 mg/kg) to tau transgenic mice (JNPL3) by oral gavage 5 days a week for 2 weeks and performed immunoblotting for total human tau and sarkosyl-insoluble fractions. There was a significant reduction in the levels of total tau and phosphorylated tau in their MB-treated mice, however, the levels of sarkosyl-insoluble tau were unchanged

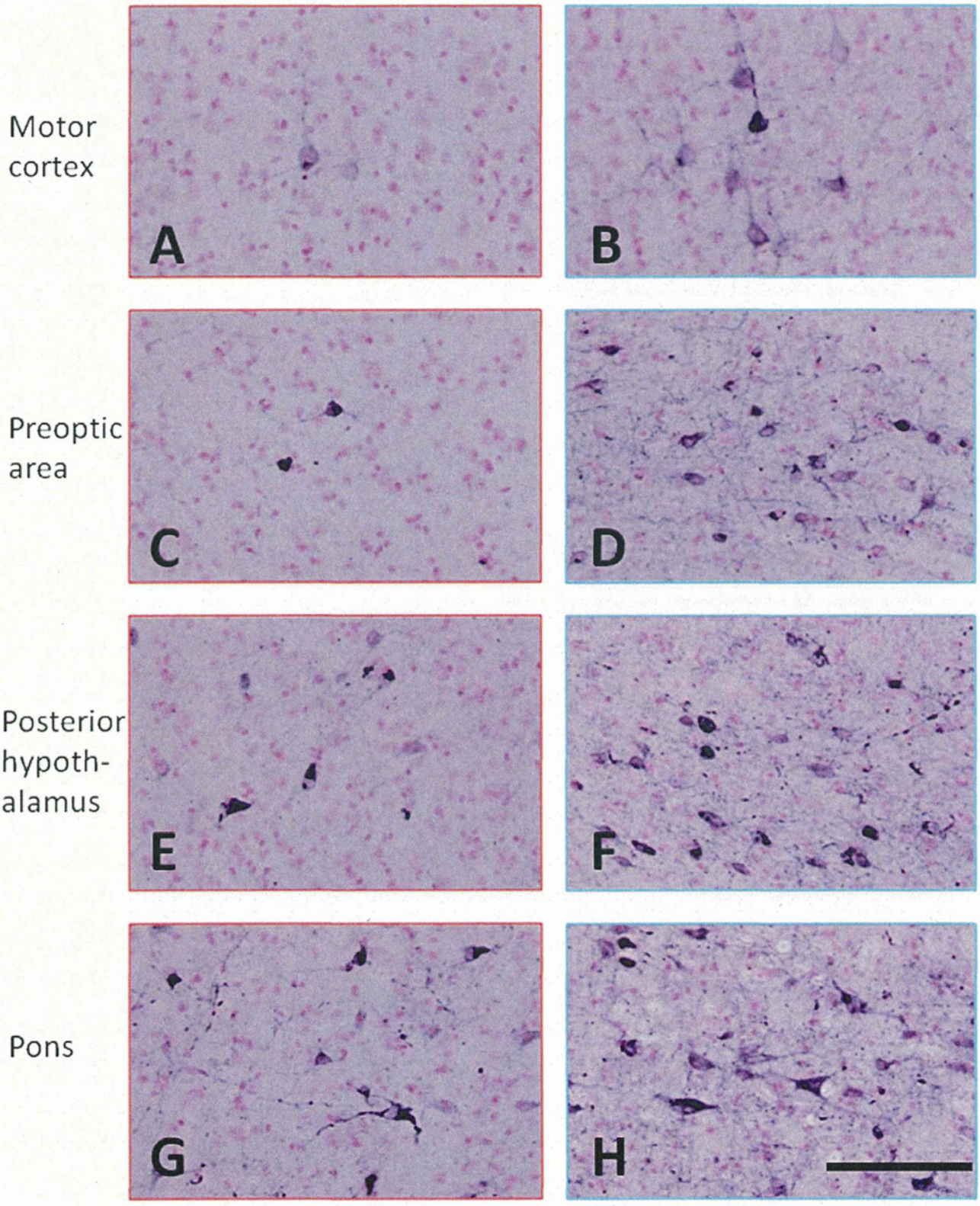

Figure 6. Immunohistochemical staining with a conformational antibody that recognizes aggregated tau. MC-1-positive neurons and cellular processes were seen in the motor cortex (A and B), prepotic area (C and D), posterior hypothalamus (E and F) and pons (G and H). A, C, E, G, mouse with a low AT8/HT7 ratio; and B, D, F, H, mouse with a high AT8/HT7 ratio. The calibration bar in H applies to all photomicrographs (50 μm).
doi:10.1371/journal.pone.0052389.g006

[7]. In the present study, the immunoblotting data revealed that phosphorylated tau was decreased in the sarkosyl-insoluble fraction after MB administration (Fig. 4). In both soluble and insoluble fractions, the amount of total tau did not differ among the three groups (Fig. 1 and 3), suggesting that the MB administration did not affect the transgenic tau expression but reduced the aggregation of phosphorylated tau. Moreover, immunohistochemical staining demonstrated that MB inhibited the spread of abnormal tau deposition from the brain stem to the cerebral cortex (Fig. 5 and 6). These immunohistochemistry findings supported the results obtained by immunoblotting.

The results of this study may agree with those by Congdon et al. in that the MB treatment reduced phosphorylated tau levels [7]. They also found reduction in the total tau levels in the total but not sarkosyl-insoluble brain fractions. While we did not examine the total brain fractions, we did not see significant changes in the levels of both soluble and insoluble tau between the MB and water treated groups. The reason for such a difference remains unknown, but it might be noteworthy that the duration of MB treatments was quite different between the two studies; we administrated MB 7 days a week for 5 months whereas they did 5 days a week for 2 weeks.

In a study by Medina et al., 0.025% MB was supplied in food to 3×Tg AD mice from 6 to 10 months of age. These mice subsequently showed reduced Aβ levels (soluble $A\beta_{40}$ and $A\beta_{42}$) and were rescued from an early cognitive deficit by an increase in proteasome activity [12]. MB improved learning and memory in these mice and the MB treatment did not affect mitochondrial function or tau pathology. In contrast, Necula et al. demonstrated that MB inhibited Aβ oligomerization by promoting fibril formation in vivo [13].

MB did not affect abnormal tau phosphorylation in a tau transgenic zebrafish model [5]. It also failed to inhibit tau and polyglutamine-protein-dependent toxicity in zebrafish, although polyglutamine aggregation was dramatically reduced. These negative results led to the conclusion that an insufficient dose of MB had been used in vivo [5]. Fertilized eggs of tau transgenic fish were cultured in a buffer containing 10^{-3}% MB. However, this transgenic model was not suitable for in vivo analysis of protein aggregation and deposition. Recently, Yamashita et al. reported that MB prevented deposition of TDP-43 in a cell culture model based on ectopic overexpression of TDP-43 [11]. These findings suggested that MB would have an anti-aggregation effect on other neurodegeneration-associated proteins.

Recent reports have indicated that MB affects the brain in many ways: it inhibits butyrylcholinesterase activity [14], inhibits noradrenalin re-uptake [15], reduces cGMP and nitric oxide [16], increases extracellular levels of serotonin (5-HT) in rat brain [12], and modulates the functions of AMPA/kainate and NMDA-type ionotropic glutamate receptors [17–18]. The beneficial effect on cognitive function observed in AD patients after MB administration may be in part attributable to its influence on the cholinergic, serotonergic and glutamatergic systems [3]. MB also improves mitochondrial respiration by shuttling electrons to oxygen in the electron transport chain, and corrects perturbations in mitochondrial metabolism induced by mutagens [19–20].

Our study suggests that MB has disease-modifying activity in targeting tauopathy involving AD. The administration of MB carried out here was very simple and could easily be applied in screening other compounds for targeting tauopathy. MB could be a leading candidate, and some MB derivatives might be exploited to develop even stronger inhibition of tau aggregation.

MB has already been used for the treatment of methemoglobinemia [21–22], septic shock [23–24], and Plasmodium infection (malaria) [25–26], which may expedite its quick approval as a potential therapeutic agent for tauopathy. While the mechanism involved remains unknown, our data suggest that administration of methylene blue might reduce abnormal tau accumulation. Finally, we did not study pharmacokinetics of MB. Congdon et al. [7] demonstrated the brain concentration of MB increased in parallel with the given doses, but this is an issue that also needs futher, more detailed exploration.

Acknowledgments

We thank Dr. P. Davies for providing MC-1 antibody. We thank Ms. Hiromi Kondo for immunohistochemical staining and Ms. Erika Arakawa for technical assistance and animal care. We also thank Dr. William Campbell and Catherine Campbell for editing of the manuscript.

Author Contributions

Conceived and designed the experiments: M. Hosokawa TA HA. Performed the experiments: M. Hosokawa MM-S. Analyzed the data: M. Hosokawa MM-S TN MY HA M. Hasegawa. Contributed reagents/materials/analysis tools: MM-S TN M. Hasegawa. Wrote the paper: M. Hosokawa TA HA.

References

1. Wischik CM, Edwards PC, Lai RY, Roth M, Harrington CR (1996) Selective inhibition of Alzheimer disease-like tau aggregation by phenothiazines. Proc Natl Acad Sci U S A 93: 11213–11218.
2. Taniguchi S, Suzuki N, Masuda M, Hisanaga S, Iwatsubo T, et al. (2005) Inhibition of heparin-induced tau filament formation by phenothiazines, polyphenols, and porphyrins. J Biol Chem 280: 7614–7623.
3. Wischik CM, Bentham P, Wischik DJ, Seng KM (2008) Tau aggregation inhibitor (TAI) therapy with Rember arrests disease progression in mild and moderate Alzheimer's disease over 50 weeks. Alzheimer's & Dementia 8: T167.
4. Gravitz L (2011) Drugs: a tangled web of targets. Nature 475: S9–11.
5. van Bebber F, Paquet D, Hruscha A, Schmid B, Haass C (2010) Methylene blue fails to inhibit Tau and polyglutamine protein dependent toxicity in zebrafish. Neurobiol Dis 39: 265–271.
6. Harrington C, Rickard JE, Horsley D, Harrington KA, Hindley KP, et al. (2008) Methylthioninium chloride (MTC) acts as a tau aggregation inhibitor (TAI) in a cellular model and reverses tau pathology in transgenic mouse models of Alzheimer's disease. Alzheimer's & Dementia 4: T120–T121.
7. Congdon EE, Wu JW, Myeku N, Figueroa YH, Herman M, et al. (2012) Methylthioninium chloride (methylene blue) induces autophagy and attenuates tauopathy in vitro and in vivo. Autophagy 8: 609–622.
8. Lewis J, McGowan E, Rockwood J, Melrose H, Nacharaju P, et al. (2000) Neurofibrillary tangles, amyotrophy and progressive motor disturbance in mice expressing mutant (P301L) tau protein. Nat Genet 25: 402–405.
9. Wolozin B, Davies P (1987) Alzheimer-related neuronal protein A68: specificity and distribution. Ann Neurol 22: 521–526.
10. Greenberg SG, Davies P (1990) A preparation of Alzheimer paired helical filaments that displays distinct tau proteins by polyacrylamide gel electrophoresis. Proc Natl Acad Sci U S A 87: 5827–5831.
11. Yamashita M, Nonaka T, Arai T, Kametani F, Buchman VL, et al. (2009) Methylene blue and dimebon inhibit aggregation of TDP-43 in cellular models. FEBS Lett 583: 2419–2424.
12. Medina DX, Caccamo A, Oddo S (2011) Methylene blue reduces abeta levels and rescues early cognitive deficit by increasing proteasome activity. Brain Pathol 21: 140–149.
13. Necula M, Breydo L, Milton S, Kayed R, van der Veer WE, et al. (2007) Methylene blue inhibits amyloid Abeta oligomerization by promoting fibrillization. Biochemistry 46: 8850–8860.
14. Kucukkilinc T, Ozer I (2007) Multi-site inhibition of human plasma cholinesterase by cationic phenoxazine and phenothiazine dyes. Arch Biochem Biophys 461: 294–298.
15. Chies AB, Custodio RC, de Souza GL, Correa FM, Pereira OC (2003) Pharmacological evidence that methylene blue inhibits noradrenaline neuronal uptake in the rat vas deferens. Pol J Pharmacol 55: 573–579.
16. Heiberg IL, Wegener G, Rosenberg R (2002) Reduction of cGMP and nitric oxide has antidepressant-like effects in the forced swimming test in rats. Behav Brain Res 134: 479–484.

17. Gonzalez-Lima F, Bruchey AK (2004) Extinction memory improvement by the metabolic enhancer methylene blue. Learn Mem 11: 633–640.
18. Wrubel KM, Riha PD, Maldonado MA, McCollum D, Gonzalez-Lima F (2007) The brain metabolic enhancer methylene blue improves discrimination learning in rats. Pharmacol Biochem Behav 86: 712–717.
19. Visarius TM, Stucki JW, Lauterburg BH (1997) Stimulation of respiration by methylene blue in rat liver mitochondria. FEBS Lett 412: 157–160.
20. Atamna H, Nguyen A, Schultz C, Boyle K, Newberry J, et al. (2008) Methylene blue delays cellular senescence and enhances key mitochondrial biochemical pathways. FASEB J 22: 703–712.
21. Kristiansen JE (1989) Dyes, antipsychotic drugs, and antimicrobial activity. Fragments of a development, with special reference to the influence of Paul Ehrlich. Dan Med Bull 36: 178–185.
22. Mansouri A, Lurie AA (1993) Concise review: methemoglobinemia. Am J Hematol 42: 7–12.
23. Schneider F, Lutun P, Hasselmann M, Stoclet JC, Tempe JD (1992) Methylene blue increases systemic vascular resistance in human septic shock. Preliminary observations. Intensive Care Med 18: 309–311.
24. Preiser JC, Lejeune P, Roman A, Carlier E, De Backer D, et al. (1995) Methylene blue administration in septic shock: a clinical trial. Crit Care Med 23: 259–264.
25. Schirmer RH, Coulibaly B, Stich A, Scheiwein M, Merkle H, et al. (2003) Methylene blue as an antimalarial agent. Redox Rep 8: 272–275.
26. Rengelshausen J, Burhenne J, Frohlich M, Tayrouz Y, Singh SK, et al. (2004) Pharmacokinetic interaction of chloroquine and methylene blue combination against malaria. Eur J Clin Pharmacol 60: 709–715.

Acta Neuropathol (2012) 124:383–394
DOI 10.1007/s00401-012-0984-6

ORIGINAL PAPER

Localization of fused in sarcoma (FUS) protein to the post-synaptic density in the brain

Naoya Aoki · Shinji Higashi · Ito Kawakami · Zen Kobayashi · Masato Hosokawa · Omi Katsuse · Takashi Togo · Yoshio Hirayasu · Haruhiko Akiyama

Received: 26 January 2012 / Revised: 2 April 2012 / Accepted: 8 April 2012 / Published online: 18 April 2012

Abstract Mutations in the fused in sarcoma (*FUS*) gene are linked to a form of familial amyotrophic lateral sclerosis (ALS), ALS6. The FUS protein is a major component of the ubiquitin-positive neuronal cytoplasmic inclusions in both ALS6 and some rare forms of frontotemporal lobar degeneration (FTLD). The latter are now collectively referred to as FTLD-FUS. In the present study, we investigated the localization of FUS in human and mouse brains. FUS was detected by western blot as an approximately 72 kDa protein in both human and mouse brains. Immunohistochemistry using lightly fixed tissue sections of human and mouse brains revealed FUS-positive granular staining in the neuropil, in addition to nuclear staining. Such granules are abundant in the gray matter of the brainstem and spinal cord. They are not frequent in the telencephalon. At the light microscopic level, FUS-positive granules are often co-localized with synaptophysin and present in association with microtubule-associated protein 2-positive dendrites. In the synaptosomal fraction of mouse brain, FUS is detected mainly in the post-synaptic density fraction. Thus, while FUS is primarily a nuclear protein, it may also play a role in dendrites. In the brains of patients with FTLD with TDP-43 deposition (FTLD-TDP), the number of FUS-positive granules in the cortex is increased compared with control cases. The increase in Alzheimer's disease (AD) is less remarkable but still significant. The dendritic localization of FUS and its increase in FTLD-TDP and AD may have some implication for the pathophysiology of neurodegenerative diseases.

Keywords FUS · Dendrite · Synapse · TDP-43

Electronic supplementary material The online version of this article (doi:10.1007/s00401-012-0984-6) contains supplementary material, which is available to authorized users.

N. Aoki · S. Higashi · I. Kawakami · Z. Kobayashi · M. Hosokawa · H. Akiyama (✉)
Dementia Project, Department of Dementia and Higher Brain Function, Tokyo Metropolitan Institute of Medical Science, 2-1-6 Kamikitazawa, Setagaya-ku, Tokyo 156-8506, Japan
e-mail: akiyama-hr@igakuken.or.jp

N. Aoki · I. Kawakami · O. Katsuse · T. Togo · Y. Hirayasu
Department of Psychiatry, Yokohama City University School of Medicine, Yokohama, Japan

Introduction

Frontotemporal lobar degeneration (FTLD) is the second most common cause of dementia in populations below the age of 65 years [7]. FTLD is characterized by behavior and personality changes, language impairment, and cognitive decline [31, 39]. FTLD comprises three clinical subtypes: frontotemporal dementia (FTD), progressive non-fluent aphasia, and semantic dementia [31]. FTD is often accompanied by motor neuron involvement [37], in which case the patients manifest features of amyotrophic lateral sclerosis (ALS), a fatal neurodegenerative disease characterized by relentless degeneration of both upper and lower motor neurons. ALS has recently become recognized as a disease that involves multiple brain regions in addition to the motor neuron system [14]. Approximately a half of patients with ALS are now known to have evidence for cognitive impairment, behavior impairment or both [36], features that resemble FTD.

Two nuclear proteins, TAR DNA-binding protein 43 (TDP-43) and fused in sarcoma (FUS; also known as translated in liposarcoma), have emerged recently as FTLD and ALS-associated proteins. TDP-43 was identified as the major component of ubiquitinated aggregates in affected neuronal

and glial cells in patients with sporadic ALS and FTLD with ubiquitin-positive inclusions (FTLD-U) [3, 34]. Subsequently, missense mutations in the TDP-43 gene (*TARDBP*) were found to be a genetic cause of a familial form of ALS (FALS), ALS10 [15, 20, 38, 40, 43], indicating that an abnormality in TDP-43 causes the disease. TDP-43 belongs to a member of the heterogeneous nuclear ribonucleoprotein family and is involved in multiple steps of gene expression, such as transcriptional regulation, pre-mRNA splicing and translational regulation [42]. In the normal brain, TDP-43 resides predominantly in the nucleus, whereas pathological TDP-43 accumulation occurs mostly in the cytoplasm or neuronal processes [3, 34].

Mutation analyses for genes having a similar structure with TDP-43 then led to the identification of mutations in the gene encoding another RNA-binding protein, FUS, in cases with FALS type 6 (ALS6) [21, 41]. ALS6 is characterized neuropathologically by the occurrence of neuronal cytoplasmic inclusions (NCIs) that have been called basophilic inclusion bodies. The NCIs in ALS6 are immunostained positively for FUS. FUS-positive NCIs have been identified in some forms of tau and TDP-43 negative FTLD. Such diseases include atypical FTLD-U, basophilic inclusion body disease and neuronal intermediate filament inclusion disease. FUS is a 526 amino acid, multi-functional protein that is involved in many aspects of gene expression [35, 44].

Now, FTLD with TDP-43- and FUS-positive inclusions are assigned as FTLD-TDP and FTLD-FUS, respectively. Subpopulations of both FTLD-TDP and FTLD-FUS are associated with ALS pathology, while mutations in TDP-43 and FUS genes cause FALS with NCIs that contain the mutated gene products. Similarities in the functions, molecular structures and subcellular localizations of FUS and TDP-43 also suggest that the pathophysiologies of these diseases are related. Like TDP-43, FUS-immunoreactivity is considered to be localized normally to the nucleus in postmortem human brain tissues, but pathological FUS accumulation occurs in the neuronal cytoplasm [5, 26, 30, 32, 33, 41]. FALS-linked *FUS* mutations that affect the nuclear localization signals (NLS) are known to cause assembly of FUS into stress granules, a type of cytoplasmic RNA–protein complexes [8, 11]. Thus, similarly to FTLD-TDP, translocation of FUS from the nucleus to the cytoplasm may play an essential role in the formation of pathological cytoplasmic aggregates in FTLD-FUS.

There is literature that describes localization of FUS to dendritic spines in primary cultured mouse hippocampal neurons [12]. Immunohistochemistry of normal mouse hippocampal tissues also demonstrated its localization to the dendrites [6]. Studies on postmortem human brain tissue indicated that, based on the amount of normal physiological staining by immunohistochemistry, the anti-FUS sensitivity was greatly influenced by the degree of tissue fixation [26, 30, 32, 33]. In the present study, therefore, we used lightly fixed, free-floating sections of postmortem human brains. We report here that, in humans, FUS is present not only in the nucleus and cell bodies but also in neuronal processes under physiological conditions. Our results demonstrate FUS-positive granular staining in the neuropil in postmortem human brain tissues. The granular staining is associated with synapses and is often located along with microtubule-associated protein 2 (MAP2)-positive dendrites. While dendritic FUS-immunoreactivity occurs constitutively in some brain regions, it is increased in the cortex of FTLD-TDP and, less markedly, in Alzheimer's disease (AD).

Materials and methods

Cases

We examined 24 cases: 9 normal subjects, 9 patients with AD, 5 with FTLD-TDP, and a patient with FTLD-FUS (for age, sex, and postmortem delay, see supplementary Table 1). No case had any family history of neurological or psychiatric disorder. Neuropathological diagnoses of AD, FTLD-TDP and FTLD-FUS were made in accordance with published guidelines [1, 10, 28, 29]. In FTLD-TDP, the TDP-43 pathology type was type A in a case and type C in the other four cases [27]. The FTLD-FUS subtype was neuronal intermediate filament inclusion disease [29]. All AD cases were studied in a previous study [4], in which they were shown to lack simultaneous TDP-43 accumulation in the amygdala, hippocampus, entorhinal cortex and temporal neocortex. For autopsied human materials, consent was obtained for every autopsy for pathological assessment and research use. This study was approved by Tokyo Metropolitan Institute of Medical Science (TMIMS) Research Ethics Committee.

Immunohistochemical staining

Small blocks of brain tissues were dissected at autopsy and fixed in 4 % paraformaldehyde (PFA) in 0.1 M phosphate buffer (pH 7.4) for 2 days in the cold. Brain regions sampled for qualitative assessment of FUS in control brain included the frontal cortex, insular cortex, hippocampus and adjacent parahippocampal gyrus, striatum, cerebellar cortex, midbrain, pons, medulla oblongata and the spinal cord. For quantitative analyses of neuropil FUS granules in control, AD and FTLD cases, hippocampal tissues containing the parahippocampal neocortex were employed. Following cryoprotection in 15 % sucrose in 0.01 M phosphate-buffered physiological saline (PBS, pH 7.4),

brain blocks were cut on a freezing microtome into free-floating sections of 30 μm thickness. For immunohistochemical staining, the sections were first incubated with 0.5 % H_2O_2 in PBS for 30 min. Sections were blocked with 10 % normal goat or bovine serum in PBS containing 0.3 % Triton X-100 (Tx-PBS), and then incubated overnight at 4 °C with the primary antibodies at the appropriate dilution. Antibodies employed in this study are summarized in Table 1. Following incubation with the appropriate secondary antibody, labeling was detected using the avidin-biotinylated HRP complex (ABC) system (Vector Laboratories, Burlingame, CA) coupled with a 3,3,-diaminobenzidine tetrachloride reaction to yield a brown precipitate.

Mice were terminally anesthetized and perfused with PBS and then 4 % PFA. Brains were removed and treated for immunohistochemistry, similarly to the human tissue sections. The mouse experiment was done in accordance with the guidelines of TMIMS and with the permission of the TMIMS's ethical committee for animal experiments.

For double labeling immunofluorescence analyses, sections were incubated overnight at 4 °C with the antibodies to FUS (HPA-008784) and MAP2, phosphorylated neurofilament or synaptophysin. These were employed as a dendritic marker, axonal marker and synaptic marker, respectively. Sections were then incubated in a cocktail of fluorescein isothiocyanate (FITC)-conjugated goat anti-mouse IgG (1:100, Millipore, Temecula, CA) and tetramethylrhodamine isothiocyanate (TRITC)-conjugated goat anti-rabbit IgG (1:100, Millipore). After incubation in 0.1 % Sudan Black, sections were observed by a confocal laser microscope (LSM5 PASCAL; Carl Zeiss MicroImaging GmbH, Jena, Germany).

Table 1 Antibodies

Antibody to	Type	Source	Dilution
FUS [1–50] (A300-302A)	Rabbit	Bethyl[b]	1:1,000 1:3,000 (WB)
FUS [1–50] (ab84078)	Rabbit	Abcam[c]	1:1,000 1:3,000 (WB)
FUS [86–213] (HPA-008784)	Rabbit	Sigma[d]	1:2,000 1:500 (IF) 1:3,000 (WB)
FUS [52–400] (11570-1-AP)	Rabbit	Prot.[e]	1:1,000 1:3,000 (WB)
FUS [400–450] (A300-293A)	Rabbit	Bethyl	1:1,000 1:3,000 (WB)
FUS [C-term] (sc-47711)	Mouse	S.C.[f]	1:200 1:500 (WB)
Microtubule-associated protein (MAP)-2	Mouse	Sigma	1:500 (IF)
Phosphorylated neurofilament[a]	Mouse	Stb[g]	1:500 (IF)
Synaptophysin (clone SY38)	Mouse	Dako[h]	1:1,000 1:500 (IF) 1:6,000 (WB)
PSD95	Mouse	Millipore[i]	1:2,000 (WB)
β-Actin	Mouse	Sigma	1:5,000 (WB)
α-Tubulin	Mouse	Sigma	1:5,000 (WB)

IF immunofluorescence, *WB* western blotting, *rabbit* rabbit polyclonal, *mouse* mouse monoclonal

[a] SMI31; [b] Bethyl, Montgomery, TX; [c] Abcam, Cambridge, UK; [d] Sigma-Aldrich, St. Louis, MO; [e] Proteintech, Chicago, IL; [f] Santacruz, Santacruz, CA; [g] Sternberger I, Bethesda, MA; [h] Dako, Glostrup, Denmark; [i] Millipore, Billerica, MA

Western blot

Fresh frozen tissue of the inferior temporal cortex from a normal subject was employed for western blot (65 years, female). To analyze the tissue distribution of FUS in the whole body, the brain, lung, liver, spleen, pancreas, kidney, heart, muscle, testes, and thymus of adult male C57BL/6J mice were used. Each tissue sample was homogenized by sonication in the lysis buffer [10 mM Tris–HCl pH 7.4, 150 mM NaCl, 5 mM EDTA, 1 % Triton, 1 % sodium dodecyl sulfate (SDS), 0.5 % sodium deoxycholate and complete protease inhibitor cocktail (Roche)]. After centrifugation at 20,000*g* for 30 min, the supernatants were collected for western blot analysis. Total protein in the lysates was quantified using the Pierce BCA Protein Assay kit (Rockford, IL, USA) with bovine serum albumin (BSA) as a standard. Western blot analysis was performed as described previously [18]. The primary antibodies were used at the appropriate dilutions as shown in Table 1.

Subcellular fractionation

The synaptosomal fraction was obtained as previously reported [17]. Further subcellular fractionation was carried out as previously described with slight modifications [9, 16]. In brief, the synaptosomal fraction was suspended in 10 volumes of ice-cold 0.1 mM $CaCl_2$. An equal volume of 2 % Triton X-100 in 40 mM Tris HCl buffer, pH 6.0, was added to incubate the sample in the solubilization buffer (1 % Triton X-100 in 20 mM Tris HCl buffer, pH 6.0) on ice for 30 min with gentle inverting. The sample was then centrifuged at 40,000*g* for 30 min. The supernatant was collected and assigned as the synaptic vesicles (SVs) fraction. The pellet was re-suspended in pH 8.0 solubilization buffer and incubated on ice for 30 min with gentle inverting. After centrifugation at 40,000*g* for 30 min, the supernatant was collected and assigned as the pre-synaptic fraction. The remaining pellet was solubilized in 5 % SDS and assigned as the post-synaptic density (PSD) fraction. The SVs and pre-synaptic fractions were combined and precipitated with chilled acetone and spun down at 20,000*g*. The precipitated protein was solubilized in 5 % SDS. Total protein was quantified using the Pierce BCA Protein Assay kit (Rockforop, IL, USA) on every sample.

Morphometric analyses

For tissue quantification, a set of sections of the parahippocampal neocortex from all cases were immunostained under identical conditions with anti-FUS antibody (HPA-008784) and counterstained with haematoxylin and the other set were stained with anti-synaptophysin. An observer (N.A.) who was blinded for the patient ID and clinical data performed both image acquisition and subsequent digital image analysis. For each case, 3 digital images (2,000 × 2,000 pixels) were captured randomly from layer II with a 40× objective and Olympus digital CCD camera (DP71). All nuclear areas stained for haematoxylin were dissected out manually, using Photoshop CS5 (Adobe Systems, Tokyo), regardless of the staining intensity for FUS. Then the number of immunopositive pixels was counted using the ImageJ/NIH Image software (http://rsbweb.nih.gov/ij/). The same threshold value was applied to all sections. The pixel counts obtained from FUS staining were divided by those from synaptophysin staining in every case. Statistical analyses were performed by Mann–Whitney *U* tests on a statistics software, GraphPad Prism version 5.0® (GraphPad Software, San Diego, CA, USA).

Results

Immunochemical characterization of FUS protein in the brain

To characterize immunochemically the FUS protein in human and mouse brains, we carried out western blot analyses using six commercially available antibodies that

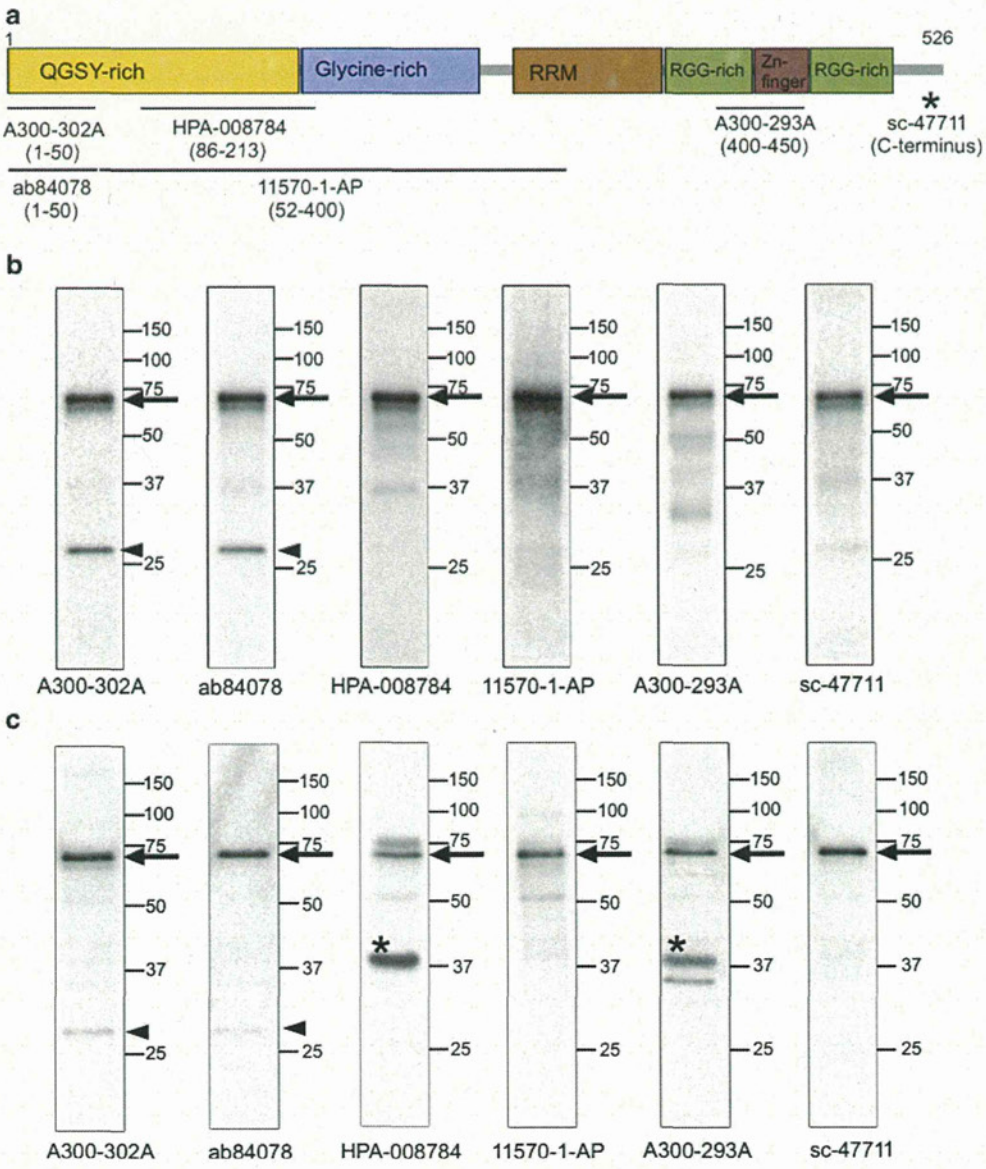

Fig. 1 Characterization of six commercially available antibodies to FUS (A300-302A, ab84078, HPA-008784, 11570-1-AP, A300-293A and sc-47711). **a** Portions of the FUS molecule used for generation of these antibodies are shown in the domain architecture of human FUS. Information was obtained from the data sheets published by each company. *Asterisk* The portion for generation of sc-47711 was not available, except for it being the carboxy-terminus. **b** and **c** Western blot with the six antibodies of an inferior temporal cortex sample from a control subject (**b**) and the whole brain of adult C57BL/6J mice (**c**). In both human and mouse, all antibodies detect a major band migrating at approximately 72 kDa (*arrows*), which corresponds to full-length FUS. Two additional minor bands at 28 kDa (*arrowheads*) and 37 kDa (*asterisks*), respectively, are also recognized by some but not all antibodies

recognize different regions of the FUS molecule (Fig. 1a). All antibodies detected a major band of 72 kDa that corresponds to full-length FUS in human brain extracts. An extra minor band of 28 kDa was detected by two anti-FUS antibodies, A300-302A and ab84078, which were raised against the N-terminal regions. We also analyzed mouse whole brain extracts. All six anti-human FUS antibodies recognized the 72 kDa major band. The two anti-N-terminal region antibodies again revealed the 28 kDa minor band. Two other antibodies, HPA-008784 and A300-293A, detected an additional minor band at approximately 37 kDa. This band was not seen in human brain extracts or in the mouse blot with anti-FUS (52-400), 11570-1-AP. The 37 kDa band, together with the 72 kDa major band, disappeared in a competition study for A300-293A with antigen peptide (Bethyl, Montgomery, TX) and by replacement of the primary antibody with non-immunized rabbit immunoglobulin (data not shown). Thus, further studies are required to clarify whether the 37 kDa band is derived from a cross-reaction to an indifferent molecule or a mouse-specific FUS fragment.

We then investigated the distribution of FUS in mouse tissues by western blot analyses (Fig. 2). FUS was expressed ubiquitously but most abundantly in the brain, lung, spleen, testis and thymus. Less, but significant expression was seen in the liver, heart and muscle and, to a lesser extent, in the pancreas and kidney. In all organs investigated, FUS was predominantly a 72 kDa protein.

Localization of FUS in control human brain

We then investigated the immunohistochemical localization of FUS in control human brains. We applied the six different anti-FUS antibodies to lightly fixed, frozen-cut free-floating sections. Consistent with previous reports [32, 33], all anti-FUS antibodies revealed predominant FUS localization to the nucleus in the cerebral cortices, together with occasional, faint cytoplasmic staining (Fig. 3a, b; Supplementary Fig. 1a, b). In addition, FUS was detected in the form of small granular structures in the neuropil of the substantia nigra pars compacta (SNpc). Of the six antibodies employed, those raised against the middle portion of FUS, HPA-008784 and 11570-1-AP, labeled the neuropil granules more intensely than the other antibodies (Fig. 3c, d; Supplementary Fig. 1c, d). We therefore employed HPA-008784 to investigate further the distribution of FUS-positive neuropil granules in various brain regions.

Figure 4a–c illustrates FUS-immunoreactivity in the cerebral cortices. In the neocortex, nuclear staining predominated over the sparsely found neuropil granules (Fig. 4a). The neuropil granules were relatively frequent in the supragranular layers compared with the deep cortical layers. In the subcortical white matter, the majority of glial nuclei were negative for FUS (data not shown). In the pyramidal layer of the hippocampal cornu ammonis (CA) regions (Fig. 4b) and the subiculum, the nuclear staining was less intense than in the neocortex, but the neuropil granules were more frequent. In the dentate granular cell layer, FUS was almost exclusively localized to the nuclei (Fig. 4c). The distribution of FUS in the parahippocampal

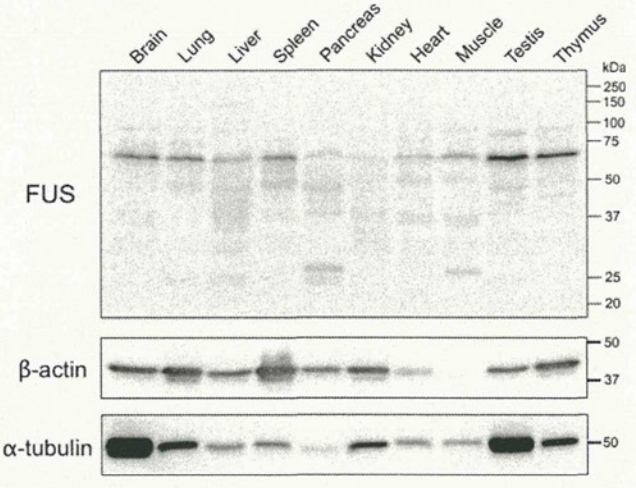

Fig. 2 Western blot of various organs of mouse with anti-FUS (11570-1-AP), anti-β-actin and anti-α-tubulin antibodies

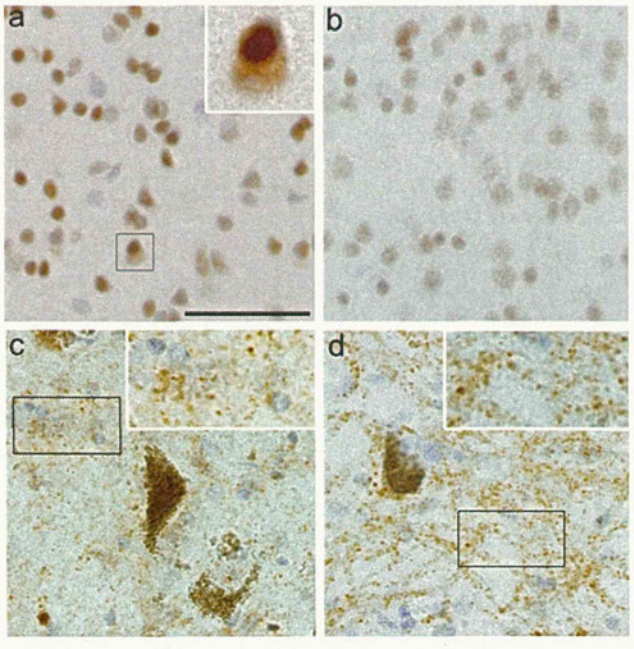

Fig. 3 FUS immunostaining of the frontal cortex (**a, b**) and the substantia nigra pars compacta (SNpc) (**c, d**) from a control subject. Antibodies used are A300-302A (**a, c**), and 11570-1-AP (**b, d**). With all antibodies, nuclear staining predominates in the frontal cortex, while neuropil granules are abundant in the SNpc. *Insets* in **a**, **c** and **d** show higher power magnification of the *boxed area*. **a–d** are at the same magnification. *Scale bar* 50 μm in **a**

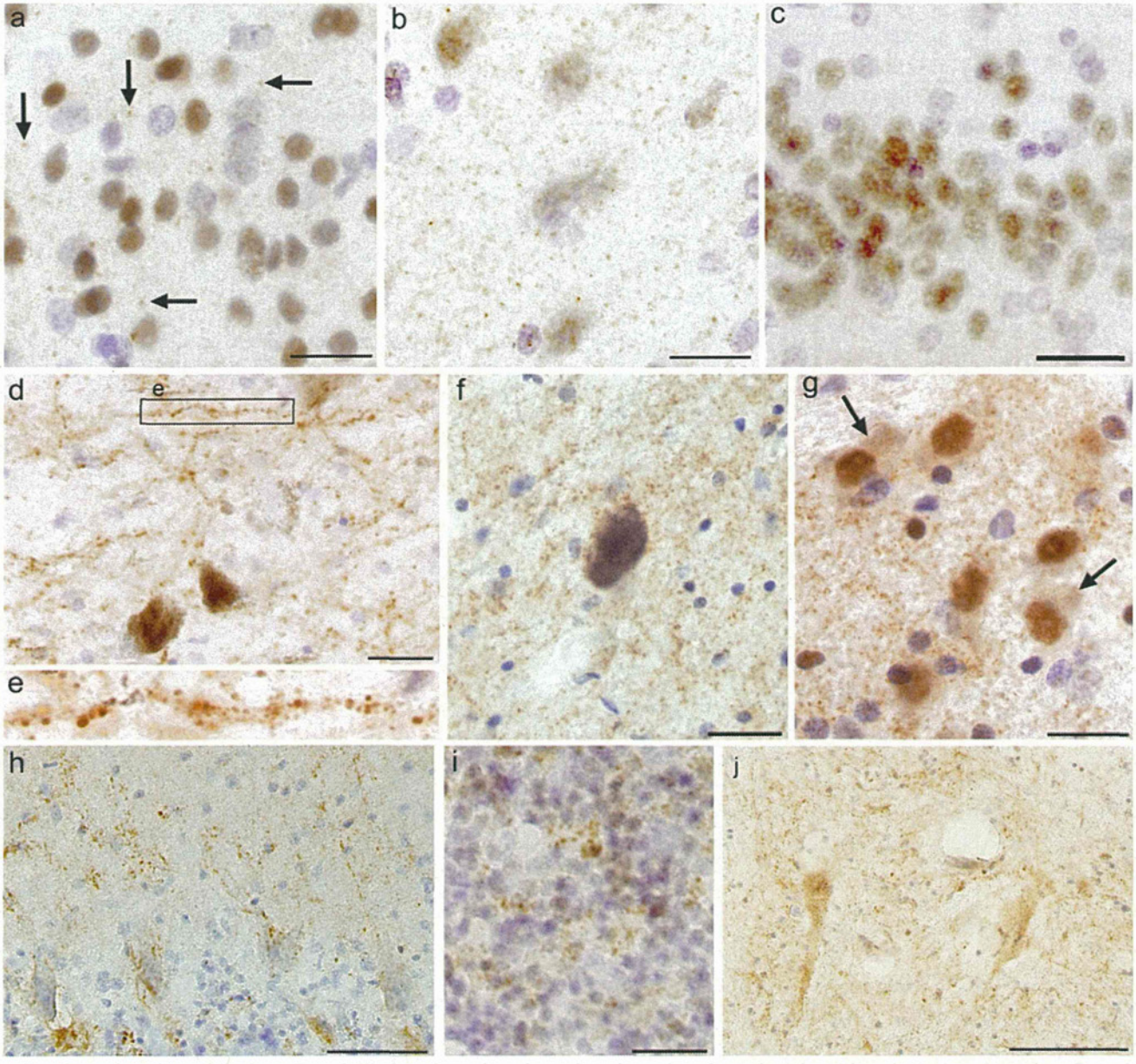

Fig. 4 Immunohistochemical staining of the control brain for FUS (HPA-008784). Layer II of the frontal cortex (**a**), the pyramidal layer of the hippocampal CA1 (**b**) and the granular layer of the dentate gyrus (**c**). *Arrows* in **a** indicate FUS-positive neuropil granules. The granular staining is more frequent in the hippocampal CA1 (**b**) and subiculum than in the neocortex (**a**) and the granular layer of the dentate gyrus (**c**). FUS-positive granules are more frequent in the brain stem: the substantia nigra pars compacta (SNpc) (**d, e**); the locus coeruleus (**f**) the pontine nucleus (**g**). The higher power photomicrograph of the *boxed area* in **d** is shown in **e**. *Arrows* in **g** indicate weak staining of neuronal cytoplasm in the pontine nucleus. In the cerebellar cortex, FUS-positive granules appear to marginate the cell body and processes of Purkinje cells (**h**). In the granular cell layer of the cerebellum, FUS-positive granules are seen with occasional FUS-positive nuclei (**i**). FUS-positive granules are also frequent in the gray matter of the spinal cord (**j**). *Scale bars* are 20 μm in **a, b, g** and **i**, 30 μm in **c, d, f** and **h**, and 100 μm in **j**

neocortex was similar to that in other areas of the cerebral neocortex.

In the caudate nucleus and putamen, FUS-positive neuropil granules were sparse (data not shown). In the SNpc, FUS-positive neuropil granules were abundant, as mentioned above (Fig. 4d). At high power magnifications, the FUS-positive neuropil granules appeared to form neuronal process-like structures (Fig. 4e). They were also abundant in the red nucleus and the locus coeruleus (Fig. 4f). In many of these brainstem areas, the majority of neuronal nuclei and cytoplasm were either negative or only faintly positive for FUS. In the pontine nucleus (Fig. 4g), FUS was localized to both the nucleus and neuropil granules. In the medulla oblongata, granular staining

predominated over the nuclear staining in the inferior olivary nucleus, while both nuclear and granular staining were evident in the hypoglossal nucleus. Weak staining was seen in the neuronal cytoplasm in the pontine nucleus and the hypoglossal nucleus. In the cerebellar Purkinje cell layer, granular FUS-immunoreactivity appeared to be located around the cell bodies and processes of Purkinje cells, the latter of which extended towards the outer molecular layer (Fig. 4h). Nuclear and cytoplasmic staining was either absent or very weak. Whether or not the FUS-positive granules were present within the cytoplasm was not determined with certainty in the 30 μm thick sections. In the cerebellar granular cell layer, only a small portion of the nuclei were positive for FUS, while granular FUS-immunoreactivity was frequent (Fig. 4i). In the spinal cord, granular FUS-immunoreactivity was abundant in the gray matter (Fig. 4j). They appeared to line along with the neuronal processes, a finding which was similar to that in the SNpc. The anterior horn cells showed diffuse nuclear and cytoplasmic staining and were overlaid by granular staining.

We then performed a semi-quantitative evaluation of FUS-immunoreactivity in the nucleus and neuropil granules in various brain regions (Table 2). FUS was mainly localized to the nucleus in the cerebral neocortices and the limbic areas. In the brainstem, cerebellum and spinal cord, on the other hand, FUS-positive neuropil granules were frequent. In such brain regions as the SNpc, Purkinje cell layer and spinal cord gray matter, FUS-positive neuropil granules were clearly observed, along with neuronal processes.

Table 2 Qualitative assessment of nuclear and neuropil FUS-immunoreactivity in multiple brain regions of control human brain

Brain region	Nuclear staining	Granular staining in the neuropil
Cerebrum		
Frontal cortex	+++	+
Insular cortex	+++	+
Hippocampal CA1	++	++
Dentate granular cell layer	+++	+
Subiculum	++	++
Parahippocampal neocortex	+++	+
Caudate nucleus	+++	+
Putamen	+++	+
Cerebellum		
Purkinje cell layer	+	+++
Granular cell layer	++	++
Mid brain		
Substantia nigra	+	+++
Red nucleus	+	+++
Pons		
Locus coeruleus	+	+++
Pontine nucleus	+++	+++
Medulla oblongata		
Hypoglossal Nucleus	+++	+++
Inferior olivary nucleus	+++	+++
Spinal cord		
Anterior horn	+++	+++

Granular staining in the neuropil: + rare, ++ frequent, but not spreading over the entire microscopic field; +++ very frequent, spreading over the entire microscopic field or neuronal processes can be identified as lining granules. Nuclear staining: + up to a quarter of the nuclei are positive, ++ a quarter to a half of the nuclei are positive, +++ more than half of the nuclei are positive

Localization of FUS in mouse brains

We next examined the distribution of FUS in the mouse brain, using two FUS antibodies (HPA-008784 and 11570-1-AP). While the instruction sheet of the antibody indicated application for mouse tissue only in the latter, both obtained positive staining for neuropil granules. In the cerebral cortex, hippocampus and striatum, FUS was localized predominantly to the nucleus. Neuropil granular staining was seen but relatively rare in those areas. This contrasted with the brainstem where FUS was present in both the nucleus and neuropil granules (Fig. 5), a finding which was consistent with the results in human brain. The distribution pattern of FUS in the nucleus and neuropil appears to be conserved throughout mammalian species.

Double immunofluorescence staining

To identify the subcellular localization of FUS-positive neuropil granules, we examined tissue sections of the SNpc and pontine nucleus from control brains by double immunofluorescence staining. In the SNpc, FUS-positive granules were present along with MAP-2-positive dendrites (Fig. 6a), but not with phosphorylated neurofilament (SMI-31)-positive axons (Fig. 6b). FUS-positive granules in the SNpc (Fig. 6c, arrows) and the pontine nucleus (Fig. 6d) were closely localized to the synaptophysin, a synaptic vesicle marker. At the light microscopic level, the association appeared to be a partial overlap (Fig. 6d: d1 and d2). FUS-positive neuropil granules seemed to be localized to synapses and dendrites.

Subcellular fractionation assay

We then performed a subcellular fractionation assay of mouse whole brain to identify the precise localization of

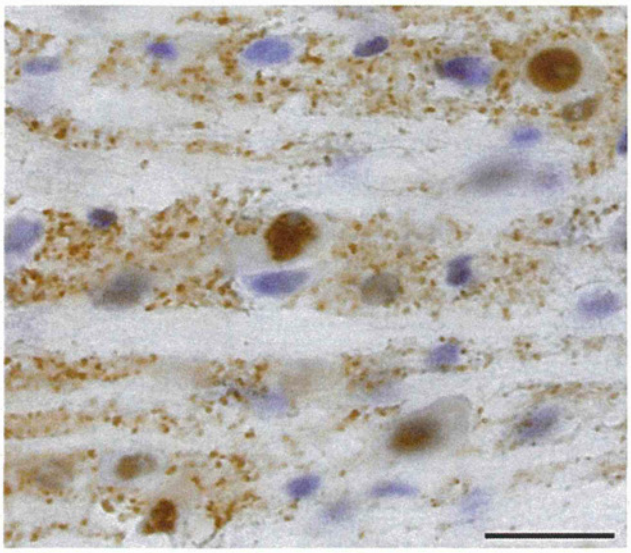

Fig. 5 Immunohistochemical staining of the mouse brain for FUS (HPA-008784). Both nuclear and granular staining is seen in the pontine nucleus. *Scale bar* 20 μm

FUS in the synapse formation. The post-synaptic density (PSD) fraction was separated from synaptic vesicles (SVs) and the pre-synaptic fraction by incubation of the synaptosomal fraction in 1 % Triton X-100 buffer and subsequent centrifugation [9, 16]. We used PSD95 and synaptophysin as markers for isolated PSD and SVs/pre-synaptic fraction, respectively (Fig. 6e). The majority of FUS in the synaptosomal fraction was sedimented to the PSD fraction and only a small amount in the SVs/pre-synaptic fraction (Fig. 6e).

FUS-positive neuropil granules increase in FTLD-TDP and AD

In addition to control subjects, we studied the hippocampus and adjacent parahippocampal neocortex of patients with FTLD-TDP and AD as well as of a patient with FTLD-FUS. FUS was not associated with senile plaques, neurofibrillary tangles or TDP-43-positive inclusions. However, FUS-positive granules appeared to be more frequent in the diseased brains than in controls (Fig. 7a, b). Tissue quantification of FUS-positive granules in layer II of the parahippocampal neocortex by computerized morphometrical analysis indicated that, following exclusion of nuclear FUS staining (Fig. 7a, b, inset), FUS-positive areas are significantly increased in FTLD-TDP ($p = 0.0010$) and AD ($p = 0.0142$) compared with control. Then the number of FUS-positive pixels was divided by that of synaptophysin-positive pixels to obtain estimate of changes in neuropil FUS granules relative to synapse density. The ratios of FUS/synaptophysin are also increased significantly in FTLD-TDP ($p = 0.0010$) and AD ($p = 0.0028$) compared with the control (Fig. 7c). These results suggest that post-synaptic FUS-positive granules are increased in some neurodegenerative conditions and that the increase is more marked in FTLD-TDP than AD. The one FTLD-FUS case showed even more FUS pixel count and higher FUS/synaptophysin ratio than any other cases (Fig. 7b, c).

Discussion

In the present study, we examined the subcellular localization of FUS in human and mouse brains. Previous immunohistochemical studies of formalin-fixed, paraffin-embedded postmortem human brain tissues for FUS showed nuclear staining in neurons and, less consistently, in glial cells, with weak labeling of neuronal cytoplasm [30, 32, 33]. Andersson et al. [2] investigated the subcellular distribution of FUS in human tissues and indicated that FUS was localized to both the cytoplasm and nucleus in most organs, but mainly to the nucleus in the brain. Other investigators, however, reported localization of FUS to dendrites and synapses in mouse hippocampal tissues and primary cultured hippocampal neurons [6, 12]. Using lightly fixed free-floating sections, we have shown that, in addition to the nucleus, a significant amount of FUS is also present as neuropil granules. By double immunofluorescence study, the neuropil FUS granules are co-localized, though often partially, with synaptophysin along with MAP-2-positive dendrites. The spatial resolution of double immunofluorescence microscopy does not permit any distinction between pre- and post-synapses [19]. The subcellular fractionation analysis of mouse brain revealed that FUS is present predominantly in the PSD fraction, indicating that the majority of the FUS-positive neuropil granules are localized to the post-synapses.

The dendritic FUS-positive granules are abundant in the brainstem and spinal cord gray matter. In control brains, they are present but not frequent in the cerebral cortex, including the hippocampus. The distribution of dendritic FUS varies significantly among brain regions, but the distribution pattern is consistent between human and mouse. The localization of dendritic FUS may be regulated by certain specific neuronal functions. Previous studies demonstrated that FUS-null primary cultured mouse hippocampal neurons exhibit abnormal spinal morphology and lower spine density [12]. It has also been reported that FUS binds to mRNAs encoding actin-related proteins, such as actin-stabilizing protein Nd1-L [13], a finding that suggests a role for the transport of mRNA to the dendrites. Together with our results, this suggests that FUS may be involved in synaptic plasticity and may regulate local translations in the dendritic spine [12, 24].

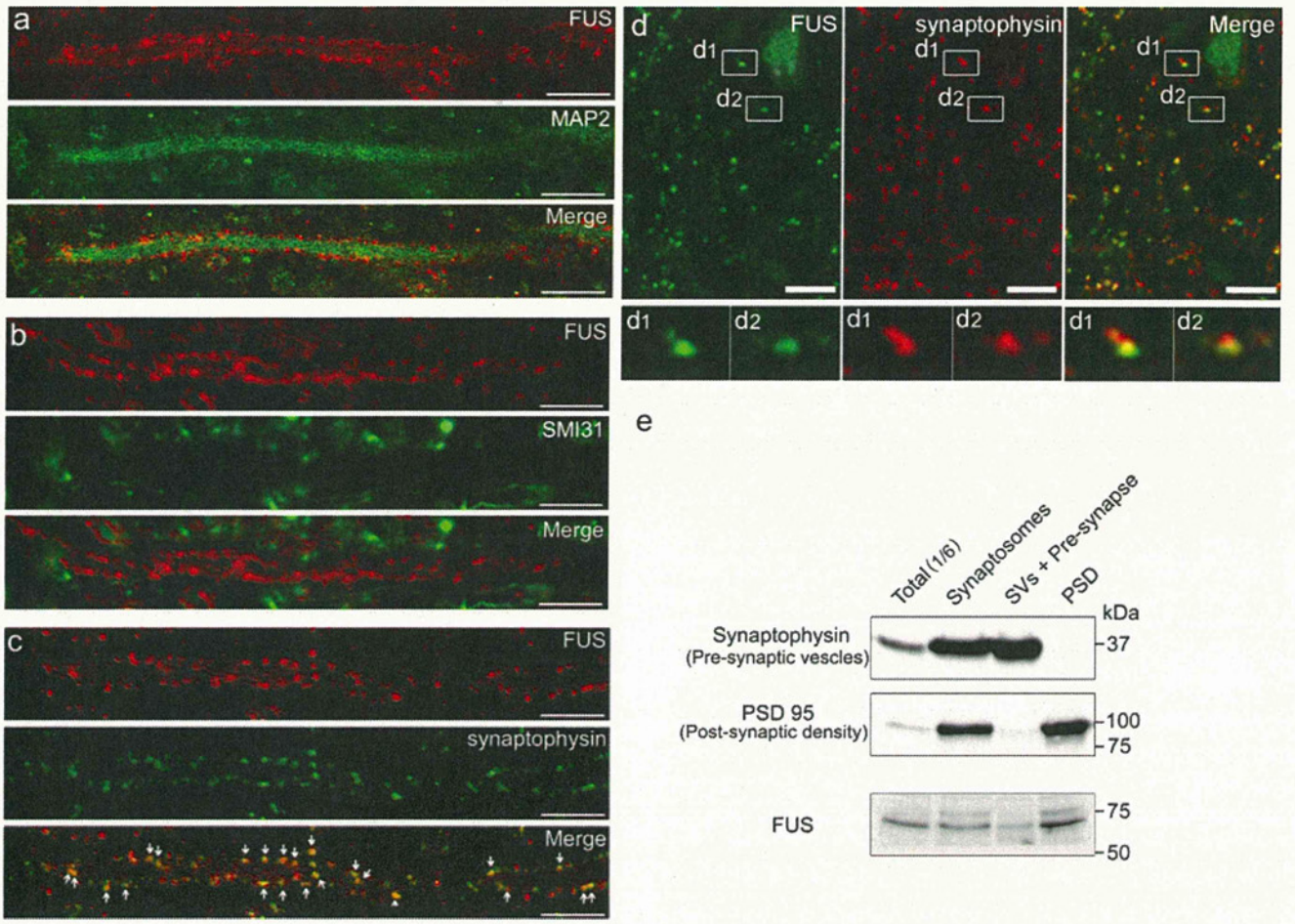

Fig. 6 **a–c** Confocal microscopic images of the substantia nigra pars compacta of a control subject. Double immunofluorescence staining for FUS and MAP-2 (**a**), FUS and phosphorylated neurofilament (**b**), and FUS and synaptophysin (**c**). FUS-positive granules are present along with MAP-2 positive dendrites (**a**) but are not associated with phosphorylated neurofilament positive axons (**b**). FUS-positive granules show close association or overlap with synaptophysin immunoreactivity (**c**, *small arrows*). **d** Double immunofluorescence staining of the pontine nucleus for FUS and synaptophysin. *Boxed areas* in **d** are enlarged in *d1* and *d2*. Scale bars in **a–d** are 10 μm. **e** Western blot of the subcellular fractions of mouse brain. The majority of synaptosomal FUS is sedimented to the post-synaptic density fraction, which is marked by *PSD95*

In western blots, FUS is recognized as a 72-kDa protein in all organs of mouse and in the human brain which is consistent with previous reports [23, 32]. The molecular weight of FUS, estimated from the amino acid sequence, is about 53 kDa, indicating that further studies are required to clarify the molecular composition of FUS [23]. In both human and mouse brain, we have also detected with two anti-FUS antibodies raised against the N-terminal region a minor band of 28 kDa. To date, any transcriptional variant corresponding to this protein species has not been found, according to the four *Homo sapiens* FUS variants in the NCBI database (NM_004960, NR_028388, NM_001170634 and NM_001170937). Moreover, the HPA-008784 antibody was raised against a FUS fragment which mostly includes the N-terminal QGSY-rich region (aa 86–213), the estimated molecular weight of which is about 22 kDa, but this antibody did not detect the 28 kDa band. Therefore, the origin of the 28 kDa band may not be the FUS protein, although the possibility remains that this band represents an N-terminal fragment of FUS.

The dendritic FUS was detected by all anti-FUS antibodies employed, but the staining intensity was different among the antibodies. Two antibodies raised against the middle region of FUS stained the neuropil granules more intensely than the other antibodies. However, given that all anti-FUS antibodies detected the 72-kDa band by western blot analyses, this may depend on a difference in accessibility to the epitopes of FUS molecule between the nucleus and the dendrites. Distinct molecular conformation or binding with other proteins, for example, could cause such a difference.

The dendritic FUS granules in the cerebral cortex are increased in patients with FTLD-TDP and, less markedly, in those with AD. Such findings suggest that the dendritic FUS in cortical neurons may be involved in some reactive or